ORNL/TM-2021/136
NFE-18-07096

A Comparative Study of Direct and Indirect Additive Manufacturing Approaches for the Production of a Wind Energy Component

Brian K. Post
Celeste Atkins
Amiee Jackson
Phillip Chesser
Alex Roschli
Abigail Barnes
Andrzej Nycz
Luke Meyer
Peter Jensen*
Martin Vcelka*
Scott Carron**

Date

Approved for Public Release.

OAK RIDGE NATIONAL LABORATORY
MANAGED BY UT-BATTELLE FOR THE US DEPARTMENT OF ENERGY

*Vestas Wind Energy Systems
**National Renewable Energy Laboratory

ORNL/TM-2021/136

Manufacturing Sciences Division

A Comparative Study of Direct and Indirect Additive Manufacturing Approaches for the Production of a Wind Energy Component

Author(s)

Brian K. Post
Celeste Atkins
Amiee Jackson
Phillip Chesser
Alex Roschli
Abigail Barnes
Andrzej Nycz
Luke Meyer
Peter Jensen*
Martin Vcelka*
Eric Putnam**
Per Jensen**
Rasmus Cardel**
Scott Carron***

*** Vestas Wind Energy Systems**

****FORCE Technology**

****National Renewable Energy Laboratory**

Date Published:

Prepared by
OAK RIDGE NATIONAL LABORATORY
Oak Ridge, TN 37831-6283
managed by
UT-BATTELLE, LLC
for the
US DEPARTMENT OF ENERGY
under contract DE-AC05-00OR22725

CONTENTS

LIST OF FIGURES

ABSTRACT

Additive manufacturing (AM) was developed in the 1980s to create three-dimensional prototypes through layer-wise approaches to fabrication. Since then, these approaches have seen improvements in both materials and processing technologies. To date, there are now 7 types of additive manufacturing processes and hundreds of materials, which can be directly printed – going directly from digital design to fabricated components. In this project, Oak Ridge National Laboratory (ORNL), Vestas Wind Systems, and The National Renewable Energy Laboratory (NREL) collaborated to evaluate the effectiveness of state-of-the-art large-scale AM processes in the production of a structural component for use in a wind turbine nacelle, through both direct and indirect manufacturing approaches.

Here, experienced AM design engineers detail techniques for AM design, including topology optimization (TO), support minimization, reverse engineering, and techniques for mitigating poor interlaminar performance. Fabrication of the components is presented, including printing parameters and postprocessing, and followed with full-scale component testing by a 3rd party testing laboratory. To evaluate the potential of the developed approaches, a complete techno-economic analysis is provided which evaluates the cost of these techniques given current and near to long-term projections of AM system capabilities.

1. PROJECT OBJECTIVES AND APPROACH

1.1 Background

The wind industry is highly competitive and depends on manufacturing very large, complex structures. Many of these structures are expensive to manufacture and have long lead times [Hughes, 2012]. The specific goal of this project is to explore the potential role of polymer and metal additive manufacturing (AM) processes in the production of a Skeleton Node (SN) component. The component functions as a joint between structural beams that carry (among other things) the electrical modules and outer enclosure. As such, the SNs experience some dynamic loads but not on a critical level. Today, the SN is a complex structure manufactured by

machining multiple metallic frames and welding the system together, requiring complicated manual interaction and documentation as demonstrated by Figure 1.

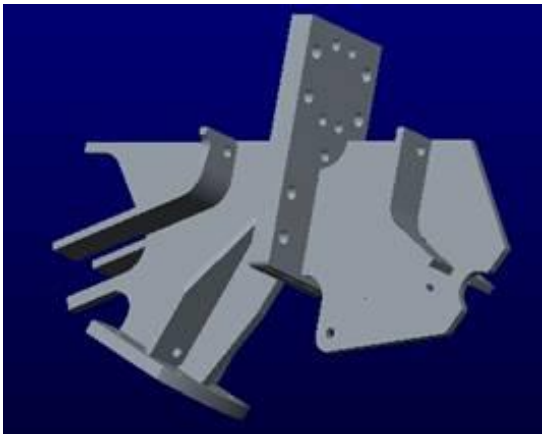

Figure 1. Example Skeleton Node

Traditional AM approaches, such as metal powder bed fusion (PBF) or blown powder directed energy deposition process (DED), have very limited build volumes that make fabrication of a component of this size either impossible or cost-prohibitive [Atenzi *et al.*, 2012]. ORNL has pioneered the development of large-scale additive manufacturing processes at the Manufacturing Demonstration Facility (MDF), including the Big Area Additive Manufacturing (BAAM) [Love *et al.*, 2020] process for thermoplastics, and the metal BAAM (mBAAM), a large-format wire arc-based DED system for the fabrication of large metal components.

In 2017 the ORNL team partnered with TPI Composites to successfully demonstrate the use of the BAAM process to produce a functional 13m blade mold set. Conservative design resulted in an outcome on par with traditional manufacturing costs for a comparable traditionally fabricated mold set, with opportunities for cost reduction in processing time and material reduction with new AM systems and a better, more optimized tool design [Post *et al*., 2017]. Analysis by NREL demonstrated a significant potential savings with the development of newer high deposition rate and large volume AM systems [Post *et al*.(2), 2017].

These processes change the economics of AM, allowing high fabrication rates with low-cost material feedstocks. If end-use components can meet application performance targets, these processes have the potential to be cost-competitive compared to conventional manufacturing processes for prototyping, limited production runs, or even full-scale production.

1.2 Objectives

The objective of this project is to explore three approaches based on additive manufacturing, to reduce manufacturing costs and lead times for large metallic/composite structures in the wind turbine nacelle. The test case will be the skeleton node (SN) which joins multiple elements together within the nacelle. The specific node was chosen by partner Vestas Wind Systems, as it is representative of production geometry for a utility class wind turbine nacelle. Using state-of-the-art large-scale additive manufacturing processes, multiple components were fabricated for the purposes of prototyping and the indirect and direct manufacturing of an end use structural skeleton node. Each end-use component was tested by a subcontractor of Vestas to evaluate the efficacy of the produced components in terms of the design loads.

In this project, we attempt to evaluate the efficacy of direct and indirect approaches to manufacturing a SN, using two different large-scale AM systems. The first approach uses ORNL's large-scale polymer AM technology to directly print the SN, using a durable and reinforced polymer material that is then infiltrated with a high-strength epoxy resin to provide structural reinforcement across layer boundaries. The second approach uses the same large-scale polymer system to manufacture casting patterns, which are then used to make a sand mold for casting a complete metallic SN (i.e. indirect application of AM to make an end use component). The final approach will focus on using a large-scale metal AM process to directly manufacture the SN.

This report details the process of fabricating the structural skeleton nodes via each approach, beginning with the establishment of loading scenarios and optimization of topology. This is followed by descriptions of the fabrication processes, including AM design of the part, fabrication rates, material consumption, and any processing anomalies. Then, the report details the testing of the produced components. The report culminates with a technoeconomic analysis to establish the economic viability of the approach, taking into consideration contemporary factors and impacts, i.e., current production rates, material costs, etc.

To ensure the reader's understanding of design decisions made by experienced AM engineers, general definitions, design considerations, and critical processing parameters for the chosen manufacturing processes are presented in the following section

1.3 Introduction to Large Scale Polymer Extrusion and Wire Metal Arc AM Processes

1.3.1 General Definitions and Design Considerations for Large Scale Additive Manufacturing

Large scale AM systems are categorized by print volumes that are at least 15 times the build volume of desktop-sized, consumer-level AM systems. Not all families of AM are well-suited to manufacture components at this scale, due to the inherent natures of their respective processes. Limitations such as unit cost of feedstock, necessity for inert or vacuum environments, and slow overall processing rates inhibit scalability. Vat photopolymerization, powder bed fusion, and material jetting are particularly suited for only small-scale AM. On the other hand, material extrusion, directed energy deposition, sheet lamination, and binder jetting have all been proven feasible at large scales; hybrid processes also play a critical role at this scale. Only these large-scale suitable families are addressed herein. Industry examples of large-scale applications for each family are provided in Table 1. Design guidelines general to the processes are then detailed, followed by unique considerations for each process applicable to the construction of a skeleton node.

Table 1. Examples of large-scale AM in industry, per AM family.

AM Family	***Industry Example***
Material Extrusion	BAAM, WinSun, Ingersoll MasterPrint, MVP Thermobot
Directed Energy Deposition	mBAAM, BeAM, EBAM, Arevo, WAAM
Binder Jetting	D-Shape, Viridis3D, Voxeljet, Desamanera
Sheet Lamination	Impossible Objects, SLCOM, Fabrisonic

1.3.1.1 Designing for End-Use: End Part Mechanical Properties

End part mechanical properties are highly sensitive to both process and material. Therefore, the AM process and material used for each part should be selected to meet the needs of the part's end use, and the part should be designed with the process and material in mind. Interlaminar bond quality draws attention in AM, as common failure modes and anisotropy originate from inadequate bonding. When selecting a print orientation, if an end part will be subjected to mechanical loads, it is important to consider that the vertical direction, perpendicular to the printed layer, of the printed part will have a lower strength (because of layer to layer interface properties). That said, methods to improve mechanical properties, such as Z-Pinning [Roschli *et al.*, 2018] or adding tensioning rods [Chesser *et al.*, 2018], have proven effective.

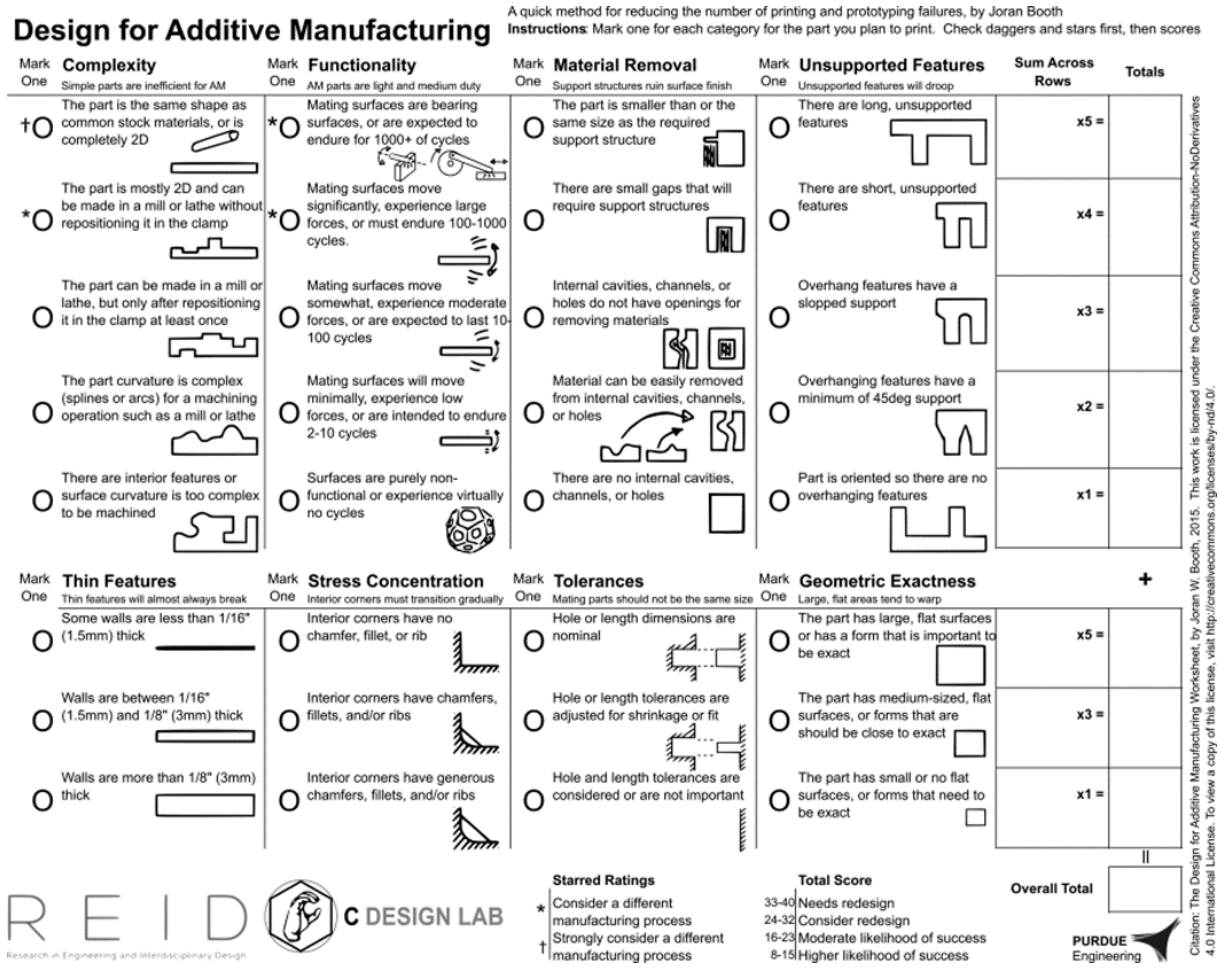

Figure 2. General design for AM considerations. From [2]

1.3.1.2 Printable Geometries

Build orientation

One major consideration in AM is the orientation of a part within the build space. Because of the layer-based approach in these processes, the orientation of a desired geometry relative to these layers can affect directional strength and the surface finish of the end part, as well as the likelihood of success in the build. Considerations when choosing the part orientation include permissible overhang angle, residual thermal stresses induced, and part application or function. Because of these considerations, part design and print orientation go hand in hand. This helps to prevent issues when pre-processing the design of the part, e.g. overhang angles and directional strength may produce conflicting orientation requirements.

Overhang angles

The overhang angle, which can be material- and process-sensitive, refers to the most aggressive angle permissible before build quality suffers. It may be referred to as relative to the vertical or horizontal axes, but the underlying concept is, particularly for ME and DED, that deposition over thin air (without any underlying support structures) is quite limited. On the BAAM system, the overhang angle limit is 45° from vertical [Roschli *et al.*, 2019], while the mBAAM system is limited to 15° from vertical [Greer *et al.*, 2019]. Areas of a part where this constraint is not met are likely to exhibit poor build quality and may cause the build to fail. As such, holes and cavities are best oriented with their cross-section in the horizontal plane or should be eliminated from the print and then added in a post-process.

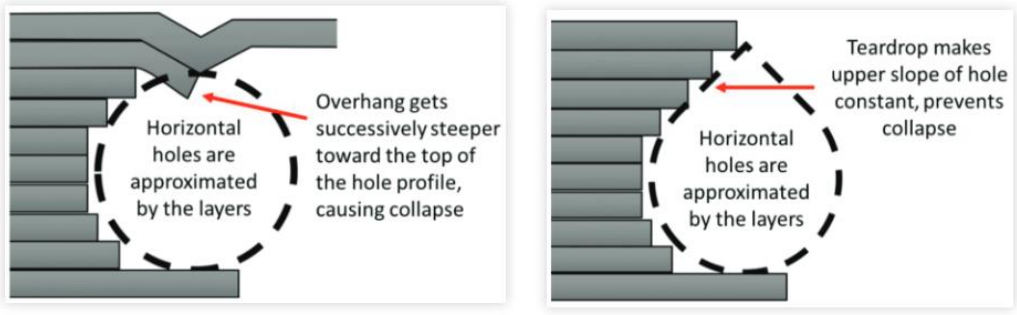

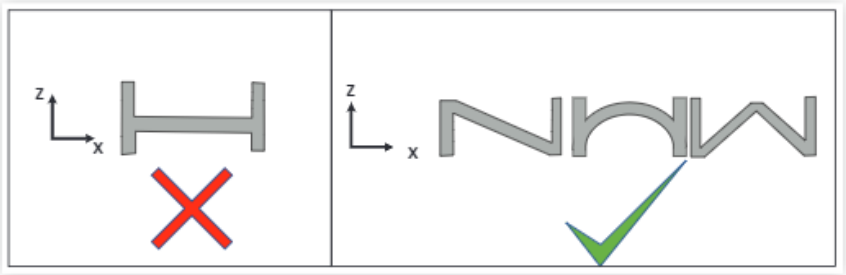

Figure 3. Top left: A circular hole oriented horizontally (parallel to the layers of the build) will often collapse toward the top. Top right: A teardrop-shaped hole can be oriented horizontally (parallel to the build layers) and is self-supporting. Bottom: Avoid flat overhangs – use slanted, arched or peaked overhangs. From [2].

Bridging

Closely related to the overhang angle is the bridging distance. While an overhang can be described as a cantilever beam with only one end supported, bridging distance refers to a beam supported at both ends but unsupported in the middle. The maximum bridging distance is closely tied to the process material. BAAM tests have indicated a maximum bridging distance between 1.85” and 2.25” for CF-ABS, depending on the nozzle [Roschli *et al.*, 2019]. Conservatively, bridging should be avoided, including in part cavities.

Support structures

Support structures are commonly used at smaller scales in ME processes to expand capabilities for overhanging and bridging geometry. However, at a larger scale, the post-processing required to remove a support structure afterward is economically prohibitive [Roschli *et al.*, 2019]. Parts should be designed and oriented to be self-supporting—such that no support structure is necessary. For the BAAM system, parts requiring support structure can be subdivided into smaller portions that do not require support structure and bonded after printing.

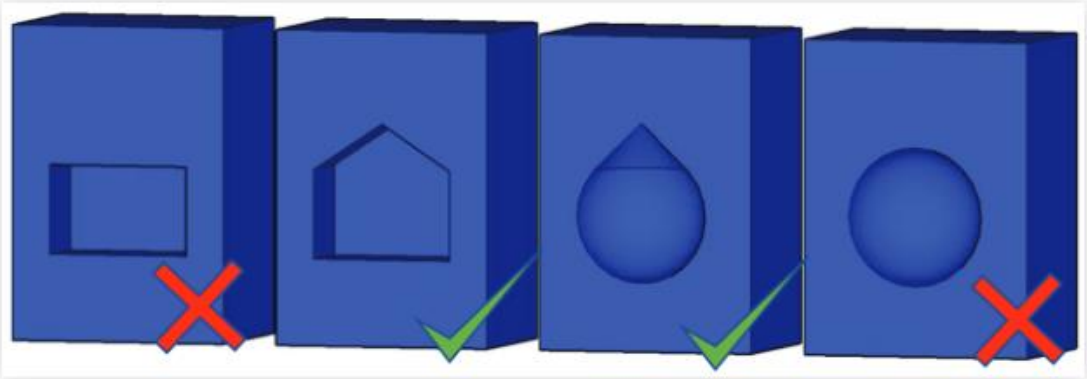

Figure 4. Cavities that are not self-supporting (far left and far right) and cavities in their modified version that are self-supporting (center). From [2].

1.3.1.3 Process Parameters & Post-processing

Build rate & bead geometry

The build rate and bead geometry are inherently related and are particularly important in large-scale ME and DED processes. Large-scale processes prioritize high deposition rates, often at the price of small features. Bead geometry describes the size and shape of an individual bead; a layer is constructed of beads. As bead geometry becomes smaller, finer feature details can be resolved in a part. However, these details come at the price of production time. On the BAAM system, bead geometry is tied to the nozzle size, but is typically 10mm (~0.40 in) wide by 4mm (~0.16 in) tall. The typical build rate is between 50 and 65 lb/hr, with a theoretical maximum of 100 lb/hr. The mBAAM system has a bead height of about 2.3mm (~0.1 in), with two parallel beads resulting in a wall approximately 12mm (~0.50 in) wide.

Layer time, bonding & residual stress

Thermal AM processes introduce residual thermal stresses into the part with cyclic thermal cycles. As a consequence, part warping or layer delamination may result from oversights in process planning. To evade these defects, the time spent on each layer (layer time) must be such that a prior layer is neither too cool nor too hot. Proper layer bonds require a layer temperature that is above a minimum temperature, while structural integrity is maintained by keeping all layers below the melt temperature. These temperature bounds and the cooling rate are dependent on the material used, the geometry under construction, and the ambient conditions of

the print. Materials can be reinforced with fibers, such as carbon fiber [Love *et al.*, 2014], to decrease thermal expansion. Geometries with a larger surface area-to-volume ratio will require a shorter layer time, while those with a smaller surface area-to-volume ratio will require a longer layer time. Best results on the mBAAM system are achieved when the layer time is minimized.

Post-processing

Post-processing refers to all steps taken after the additive process is complete, to achieve part functionality. Machining, polishing, or heat treatment are all examples of potential post-processes. It is recommended to design with post-processing in mind, whether that be tool accessibility for machining or overbuilding the part to near net shape such that high tolerance mating surfaces can be achieved. Large scale processes typically target a near-net geometry and require post processing for surface finish, tolerancing, or feature addition (holes).

1.3.2 Prototyping, Direct, and Indirect Uses of Additive Manufacturing

There are three primary contemporary use cases for additively manufactured components. Listed in order of industrial adoption, these methods are prototyping, indirect, and direct manufacturing. While each has merit, the industry trend has been to push towards direct manufacturing of end use components. This trend follows the change in nomenclature of the industry itself from “rapid prototyping” in the 1990’s, to “3D printing” in the early 2000’s, and finally to “additive manufacturing” which is now used interchangeably with 3D printing. While the properties and geometric capabilities of the processes have continued to advance to the level that some direct replacements of production components have been developed in industries like aerospace, there has been limited adoption in more traditional manufacturing sectors. Industries like heavy manufacturing or automotive have seen very few successful direct-use AM solutions, primarily attributable to production rate and economic issues of the current systems.

Prototyping has long been the target for polymeric AM systems, allowing production engineers to fabricate early protypes to test the three F’s: form, fit, and function. AM shortens the design cycle, allowing the development of more solution variants and short-circuiting the heavy investments that are required to make the first article in production tooling. While the materials, performance, per unit cost, and finish of the produced article is generally inferior to the that of the production part, the value of an early prototype has driven the AM industry, and is

the primary reason for the explosion of AM systems across manufacturing enterprises. In recent years, with the expiration of some of the foundational patents of the extrusion-based AM processes, the material selection, machine varieties, and capabilities have been greatly expanded by the entrance of competitors in the marketplace.

With advancements in materials and processing technology, indirect manufacturing using AM components has become more prevalent. Items like production tooling, jigs and fixtures, and assembly guides are ideal application cases for AM because they emphasize complex features, limited quantities, and stiffness rather than strength-limited performance requirements. Large-scale AM and hybrid strategies hold promise to reduce lead times for tools like casting patterns, compression molds, and injection molds, but lack the empirical data and subjective examples necessary to achieve trust within the larger industry. These problems only intensify when pursuing direct AM of end-use components in strength-limited applications. Often, the only way to achieve necessary certification is through proof testing or statistical analysis of significant numbers of destructively-tested component samples.

2. OPTIMIZATION OF THE TOPOLOGY OF THE SKELETON NODE

Topology optimization (TO) is a computational design methodology that optimizes the material within a structure given a known set of loads, boundary conditions, and constraints with the goal of maximizing performance while simultaneously reducing component weight. Several optimization tools and methodologies were trialled to capture the differences and synergies between each approach. To physically verify some of the assumptions, the scope included physical full-scale builds of the designs, which were compared to a standard Wind Turbine Generator (WTG) nacelle structural node/section. Three manufacturing processes were targeted: welding, casting and AM. The AM portion of this study involved the use of both metallic and composite materials to realize an optimized design. The baseline component was taken from a node component of an upcoming design planned for release in 2020.

To simplify the optimization studies, a single operational load case was chosen to represent a typical loading scenario. The fatigue criteria and other lifecycle load cases such as transport and installation were not included in this study. The specified loading conditions can be seen in Figure 5, where the extreme tensile values for this particular load case were only design driving in some areas of the component. Hence, it is important to note, that some features of the

geometry (such as thicknesses and flange sizes) may have been overdesigned for this particular load case, due to other design-driving load cases.

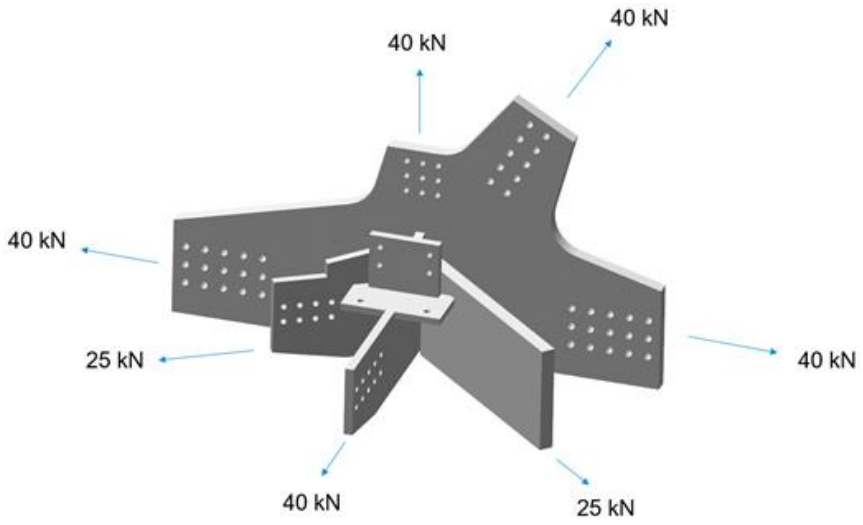

Figure 5. Node component load condition and magnitude

There were several approaches and software that were trialled to define an optimization workflow:

- Ansys internal optimization module
- Autodesk generative design, (volume optimisation)
- Optistruct (topology optimization)

Initially, ANSYS was used due to its compatibility with current workflows. All models and analyses were conducted using either the Ansys Parametric Design Language (APDL) and/or workbench, combined with scripting for specific functions. The optimization features, however, were basic in their implementation at that time and the results did not yield significant reductions in weight/volume. One advantage was that manufacturing criteria, such as draw direction, could be included.

In this case, only the interfaces from the existing geometry and the load vectors were used. A design space volume was constrained, and the output was a geometric model fulfilling the required loads in the specified volume. The challenge to set up this kind of analysis was that the constraints had to be placed in such a way as to represent the component as a system, due to the

interaction of loads in all directions simultaneously. Using a script, a ‘weak springs’ approach was used to allow sufficient convergence.

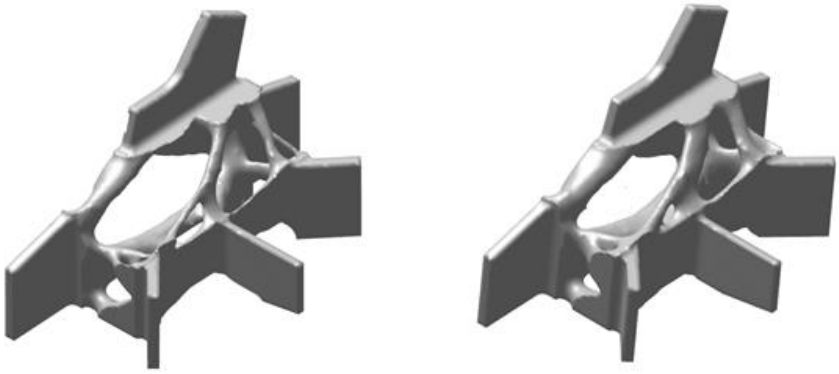

Figure 6. Node optimization results using the ANSYS internal optimization design approach.

Autodesk generative design software was used to facilitate a similar approach; however, in this case, specific nodes in the centre of the geometry had to be constrained to enable a viable solution. The results produced by this approach differed from those of the native ANSYS optimization tool. The output geometry is shown in Figure 7. The software at the time (version 2018) was less mature than the ANSYS tool and did not allow thorough enough control of the optimization constraints. The features have grown significantly since then but have not been benchmarked again. A recommendation would be to re-evaluate with the current feature set, to establish the level of improvement and any changes to the result.

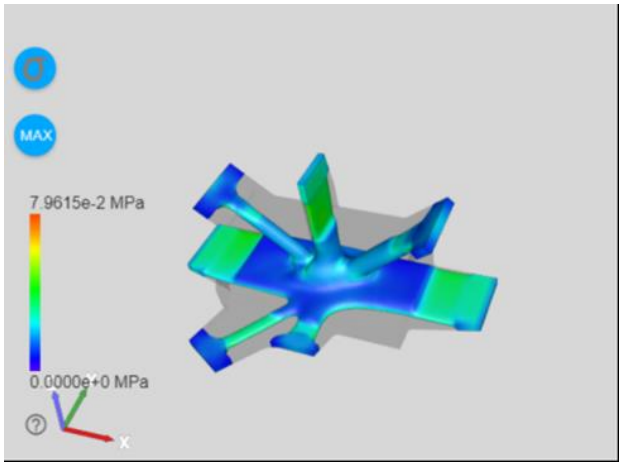

Figure 7. Node optimization geometry using Autodesk generative design.

The final approach was to use the baseline geometry inside Optistruct and allow a volume optimisation constraint to drive the optimization. Here, only the original volume of the node could be used as the design space. The reduction in weight amounted to a range between 40%-50%. Two different levels of material reduction are show in Figure 8. One advantage when using this software was the ability to map the stress path in one single approach. In the previous approaches/software, these steps had to be done independently. Several screenshots that show the dominant stress path are presented in Figure 9.

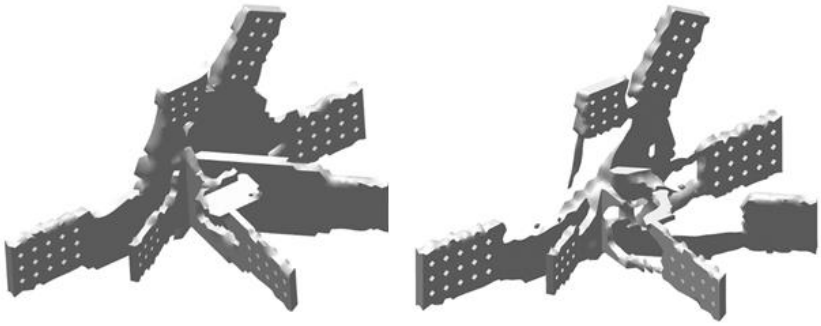

Figure 8. Node optimization results using Optistruct.

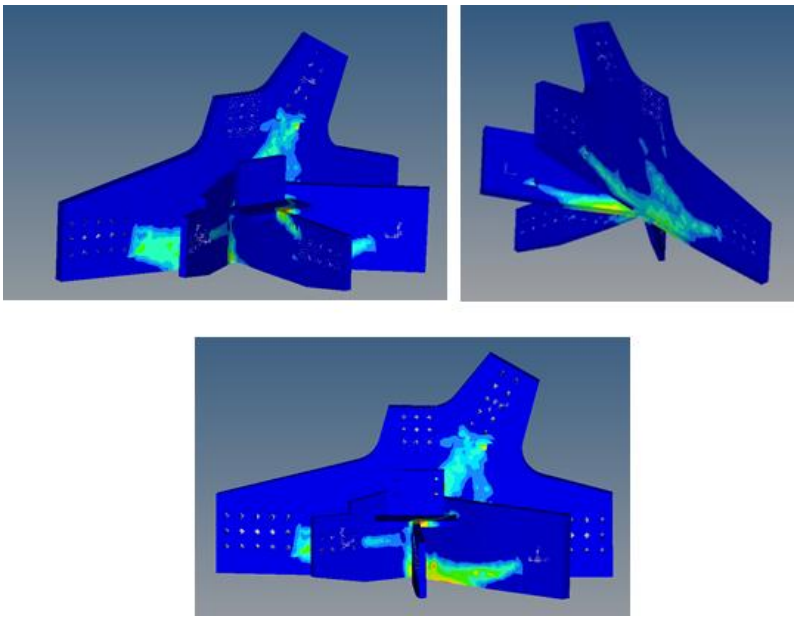

Figure 9. Various views of stress distribution and flow path mapped across the original node design.

The result of a TO is generally a surface mesh geometry showing the "ideal" geometry of the component, minimizing the weight by removing all material not contributing to the support of the design loads. This is generally constructed with no regard to the constraints of the manufacturing processes themselves, or the desired print orientation and any anisotropic effects resulting from the in-situ process dynamics. The following sections describe the process of Computer Aided Design (CAD) reconstruction and fabrication of the topologically-optimized SN for the 3 chosen fabrication approaches, direct thermoplastic print with secondary reinforcement, casting using a thermoplastic printed pattern, and direct metal print.

3. ADDITIVE MANUFACTURING OF A TOPOLOGY-OPTIMIZED COMPOSITE SKELETON NODE

3.1 Manufacturing Process: Large Scale Composite Material Extrusion via BAAM

Material extrusion forces feedstock material through a fine orifice to form beads while traversing the path of a layer. Thermoplastic polymers are the most common materials, although foams, thermosets, composites, and paste-like materials such as chocolate, concrete, or clay are also processed in this manner. Surface finish is generally correlated to total build size due to the economics of processing time; that is, as build size increases, surface finish and minimum feature size deteriorate.

Mechanical properties are generally anisotropic due to the limitations in interlaminar adhesion, subject to the physical constraints of the material's solidification dynamics. For example, when thermoplastics are heated, the polymer chains relax, allowing the material to flow and the chains to entangle. As the material cools, it solidifies, and the polymeric chains tighten. This ultimately develops the compressive strength necessary to support the subsequent layers, at the expense of the ability of the polymeric chains to entangle across layer boundaries, resulting in weak layer interfaces. If the material is kept significantly above the glass transition temperature, good interlaminar performance is possible, but the weight of the subsequent layer(s) and the extrusion forces can cause deformation and collapse of the structure. Contrarily, if the temperature at the interface is well below the glass transition temperature, the subsequent layer(s) are well supported, but the bond strength is so low that forces induced by the contraction

of the material from its molten to solid phase transition can cause delamination at the interface and failure of the part. There exists, therefore, an optimal layer time and temperature processing window that bounds the object geometry, the deposition rate, and the layer time for a given part.

The BAAM, developed by ORNL in partnership with Cincinnati Inc. and shown in Figure 10, is capable of printing composite materials to create parts up to 8ft x 20ft x 6ft in volume. These composite materials are typically comprised of a neat, matrix thermoplastic with a fiber reinforcement. This reinforcement serves two primary purposes: 1) to increase in-plane strength and stiffness (with a high length to diameter ratio L/D, the fibers contribute significantly to the material properties of the composite material), and 2) to reduce the macro coefficient of thermal expansion (CTE) of the material, which helps control warping of the printed part [Love *et al.*, 2014]. As each layer transitions from its molten state to its solidified state, residual stresses are formed and transferred to the previous layers. These stresses continue to build as the full component is fabricated, resulting in deformations and delamination. The fibers reduce the CTE of the material, and thereby limit the shrinkage and reduce the residual stress formation, resulting in more dimensionally stable printed parts.

Figure 10. Cincinnati BAAM Used to print the composite AM Nodes and Casting Patterns

The SN being printed for this project is a small component by BAAM standards, and therefore could not be printed at the maximum deposition rate because of the processing

dynamics. Each part was printed out of a Carbon Fiber-reinforced Acrylonitrile Butadiene Styrene (CF-ABS) with 20% carbon fiber by weight, a standard medium-performance engineered thermoplastic commonly used in the BAAM process.

3.2 Design of Composite AM Node

The output of the Ansys topology optimization (TO), performed by Vestas, was a mesh file in the form of a STL (a stereolithography file format). These formats are compatible with slicing engines and commonly used for additive manufacturing, however, the results from the topology optimization neglect the design for additive manufacturing (DFAM) constraints imposed by the material extrusion process, i.e. minimum support angles, bridging distances, minimum profile widths, etc. In order to accommodate these constraints, the surface mesh must be converted into a parametric CAD model. Unfortunately, while many CAD companies are working on automated tools to accomplish the conversion of TO results to parametric CAD, these tools are very primitive and most reconstruction remains a manual process. The designer utilizes standard CAD operations, typically combinations of boss extrusions (where a 2D profile sketch is extruded to form a 3d shape), lofts (where multiple 2D sketches are connected with spline boundaries to create 3d shapes), and sweeps (where a 2D profile is swept along a guide curve to form a 3d shape) to recreate approximations of the TO geometry. This manual reconstruction process is tedious, and most of the steps are therefore left out of the following discussion, but the essential operations are discussed.

The result of this reconstruction is illustrated, overlayed with the STL, in Figure 11. The opaque black object is the STL and the transparent grey object is the manually-reconstructed parametric CAD design.

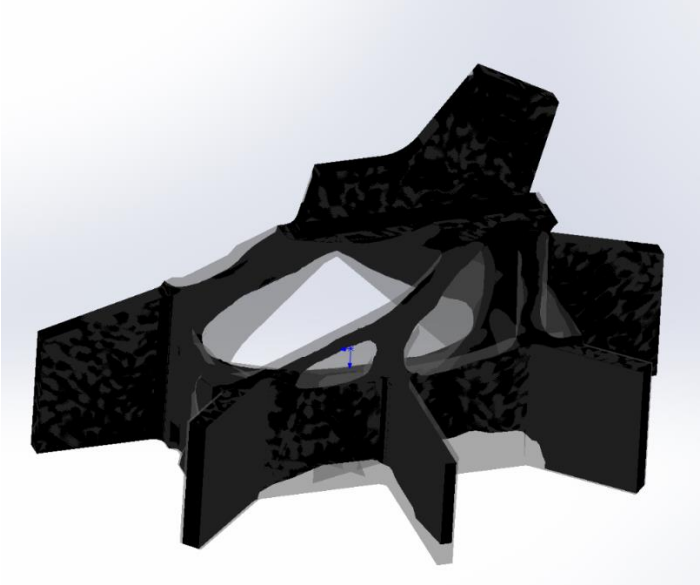

Figure 11. Overlay of ANSYS internal optimization node result and printable AM component

First, the STL was imported into a parametric CAD program (SolidWorks by Dassault Systemes). Using an add-in package (Geomagic for Solidworks), the STL was dissected to create construction planes for each of the boss features, and normal to the TO struts. Each boss was extruded one feature at a time, to form the connection tabs of the SN.

The organic struts were each reconstructed from cross-sections extracted from the STL by the Geomagic add-in. Simplifying geometry was used to approximate the profile construction geometry. An example is shown in Figure 12. Note the circular cross-sectional profiles were replaced with tear drop shapes that terminate on the build surface, with profile widths equal to two bead widths (0.68” for a 0.3” nozzle diameter). This results in self-supporting geometries for the struts. In the case where struts were located far above the build surface, the profile was tapered at 45degrees to the thickness of 2 bead widths, and then held constant until the profile met the build surface. If the area of the profiles along the length of the strut varied significantly, a loft operation was used to create a solid body that was then merged into neighboring features, as shown in Figure 13.

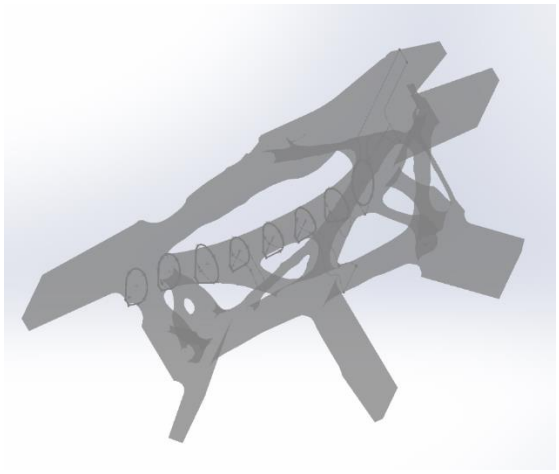

Figure 12. Reconstruction of structural member via loft from approximated profiles extracted from cross-sectional sketches

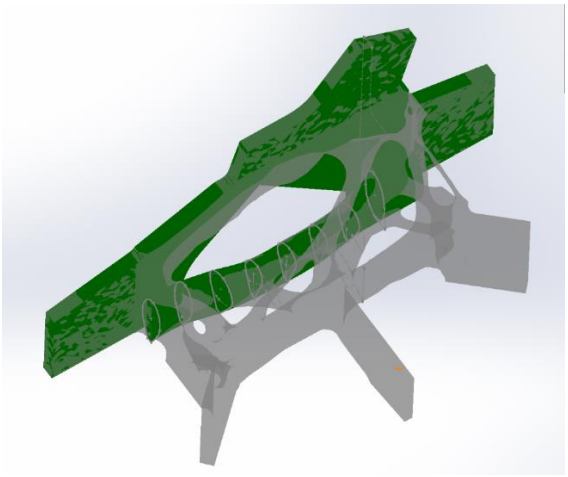

Figure 13. Merging lofted and extruded features to create reconstructed geometry

For struts with a relatively consistent cross-sectional area, conservative sweeps were used, using a design curve approximating the midline of the desired strut, as shown in Figure 14. Again, instead of a circular swept profile, the teardrop shape was used, and connected with a two-bead wall that extended downward to the build surface to form self-supporting geometry.

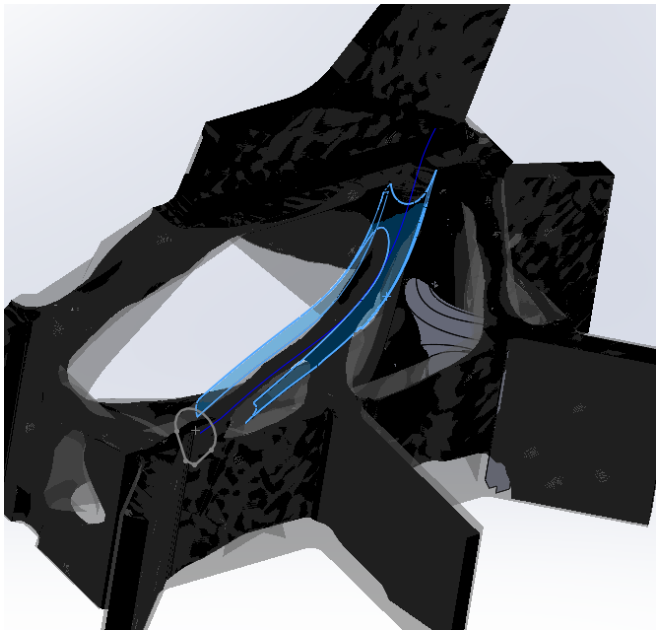

Figure 14. Sweep operation to create reconstructed strut geometry

While some holes are achievable with support, or with an inverse teardrop shape (an example of which is in the rear of the SN), it is typically faster and more structurally sound to simply reduce the profile width within a part, to reduce mass through a section represented by a hole in a TO result unless the hole is large and represents a significant weight savings. Take for example the hole presented in Figure 15. This hole would cause two separate printability issues. One is an unsupported overhang. The other is a disconnection between islands, which would increase print time, create an open edge where crack initiation points could form, and create small profiles which cool faster than the surrounding material causing poor interlaminar bonding. Therefore, the area in blue was embossed into the existing wall to create a reduction in cross-sectional area without forming a complete hole through the profile.

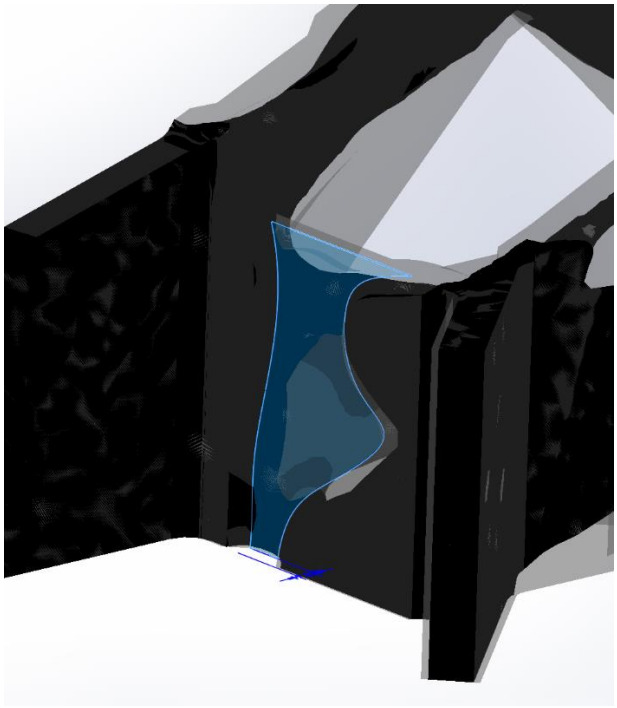

Figure 15. Approximating holes in boss geometry for printability optimization

The printable BAAM SN Node is the result of repeated boss, loft, sweep, and cut operations, as described, and the result is shown below in Figure 16, next to the result from topology optimization. A second version was fabricated to create a completely hollow inner chamber, which will be described in the relevant subsection.

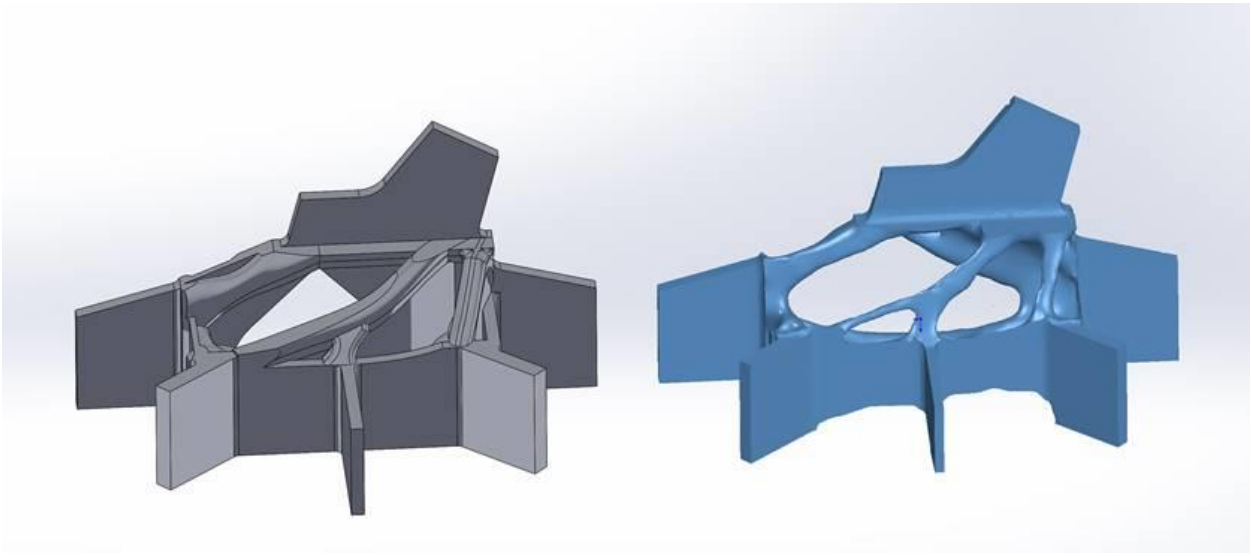

Figure 16. Design for the TO printable SN composite node V1

3.2.1 Fabrication of Iteration 1. – Sparse Fill Hybrid Composite Node

Printed Part Weight: 78.7lb

Print Time: 7h 20m

The first iteration of the Composite Printed SN (after the first solid geometry prototype, which was used to calibrate the testing equipment) was printed as a sparse-fill interior component. A single outer perimeter formed a geometric shell, of which the interior was filled with alternating lattice.

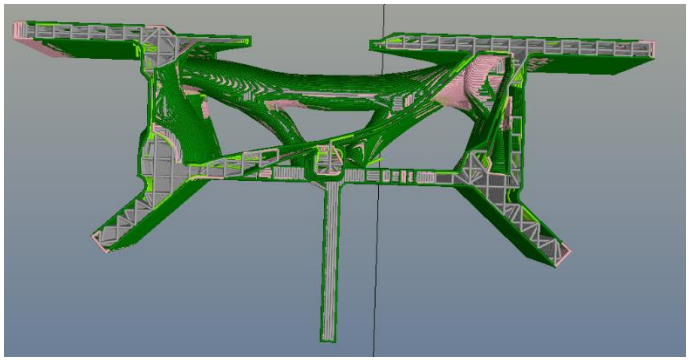

Figure 17. V1 Composite SN with sparse alternating internal lattice

Printing occurred on the BAAM system, as shown in Figure 18. Upon removal, the internal volume was filled with high-strength epoxy resin. The resin used had a low viscosity, allowing it to flow around all the internal lattice features and provide a continuous matrix material across layer boundaries, to improve the interlaminar strength and fill porosity within the part.

Figure 18. Printing the V1 Composite structural node

Attempts were made to incorporate long-strand carbon fibers (>0.5” in length) to improve the mechanical properties of the infill structure, but the added fiber increased the viscosity and thus prevented the flow of material into the internals, so the approach was ultimately abandoned. After curing, the flanges were machined to support the grips of the test apparatus.

3.2.2 Fabrication of Iteration 2. – Core and Shell Composite Node

Printed Part Weight: 74.3lb
Print Time: 6h 15m

Version two of the composite node comprised of a minor set of design changes to allow the SN to be printed as a completely hollow shell structure, to be filled with high-strength epoxy resin. This required not only the external surfaces to meet the 45-degree overhang rule to avoid support structures, but the internal surfaces as well. The hollow shell design also eliminated starts and stops which dramatically reduced the print time with only a slight reduction in printed weight. An example of a single sweep operation used to modify the geometry of the SN is shown in Figure 19.

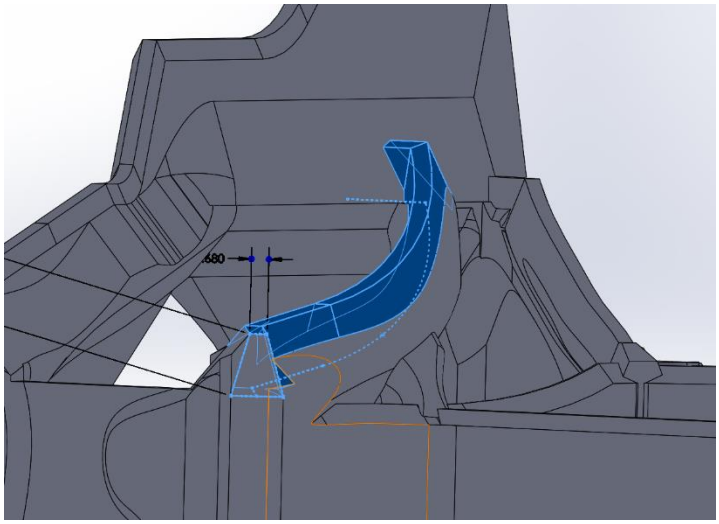

Figure 19. Swept feature to allow unsupported hollow interior spar

All of the blue features in Figure 20 were added to eliminate internal overhangs >45 degrees in the V2 composite SN. In doing so, the internal volume of the node was expanded,

requiring more epoxy, but eliminating porosity and voids in areas where epoxy was unable to flow in V1.

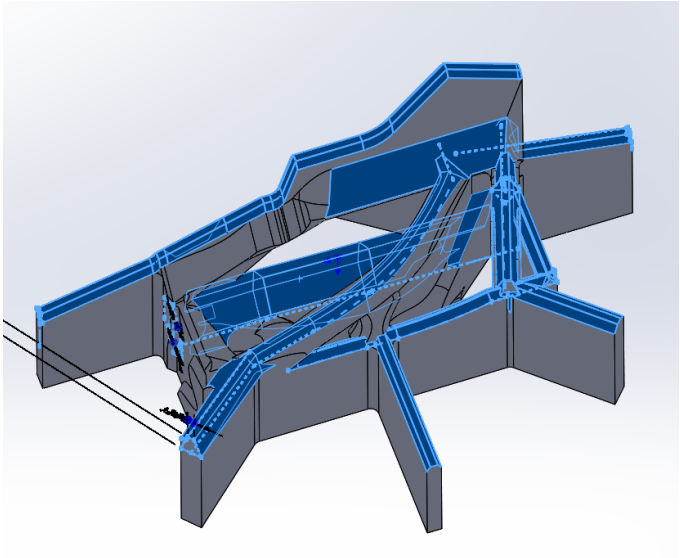

Figure 20. Modified features from V1 to V2 composite SN

While printing V2, the hollow structure near the top flange led to extremely low layer times, and without internal bracing structures, the flange collapsed under the weight of the deposited material and extrusion forces. Even with manual intervention, i.e. slowing the deposition rate on the final layers, it was too little, too late to preserve the flange feature. However, because this flange was not included in the testing apparatus, the decision to finish the component was made, the top was sealed with structural adhesive and the core was filled with high strength epoxy resin. Figure 21 shows the final as machined V2 composite node.

Figure 21. Complete V2 printed composite skeleton node

4. ADDITIVE MANUFACTURING OF TOOLING FOR A TOPOLOGY-OPTIMIZED CAST METALLIC SKELETON NODE

4.1 Manufacturing process: Sand casting via a BAAM-printed casting pattern and core boxes

Printed Part Weight: 2118lb
Print Time: 93h 5m

Sand casting involves a replica of the exterior of the cast part, split in half down a parting line; this is called a foundry pattern. Foundry patterns are usually made of wood and placed on a backer plate that has locating features. A box is built around the corners of the backer plate. Sand is packed into the box around the pattern, forming the mold. This is repeated for both sides. In the casting orientation, the top half is called the cope, which has riser and runner pins to pour the metal in and let the air inside escape. The bottom half is called the drag. Sometimes, the pattern creates cavities that are not included in the part and therefore are not meant to be filled with material. To solve this issue, core boxes are made. These boxes create blocks of sand that fill in the undesired cavities. The cores are supported between the cope and drag. Once any cores are placed in the drag and the cope is set on top, the riser and runner pins are removed, and the molten metal is poured into the runner channel. The material that solidifies in the runner and rise must be cut off the part in post-production. This entire process is summarized in Figure 22.

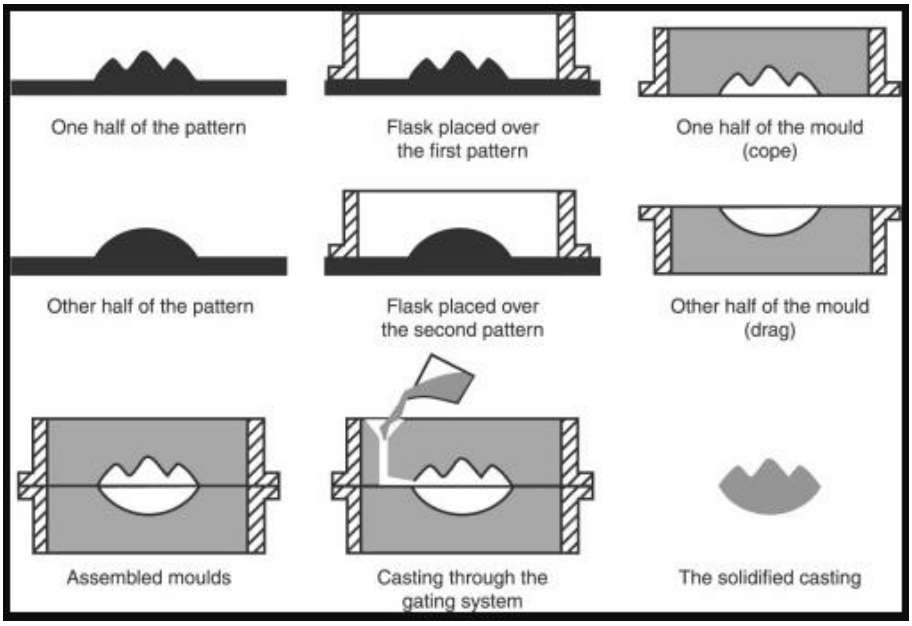

Figure 22. Casting Overview Diagram [Otarawanna *et al.* 2011]

For our purposes, the casting pattern was manufactured with the same printing process as the composite node discussed in Section 3.1. Six large parts were printed on the Cincinnati BAAM out of 20% carbon fiber-reinforced ABS, and two smaller parts were printed on the Fortus 900 out of Ultem. The Fortus 900 is a small-scale printer with a build volume of 36” x 24” x 36” and uses filament-based feedstock, unlike the BAAM, which uses pellets.

4.2 Design of Cast Component

Topological data of the structural node (SN) from Vestas was provided in an STL file, as previously mentioned. It was imported into a parametric CAD program (SolidWorks by Dassault Systems), and then the node was manually reconstructed by creating planes, sketches, and extrusions using vertices of the mesh.

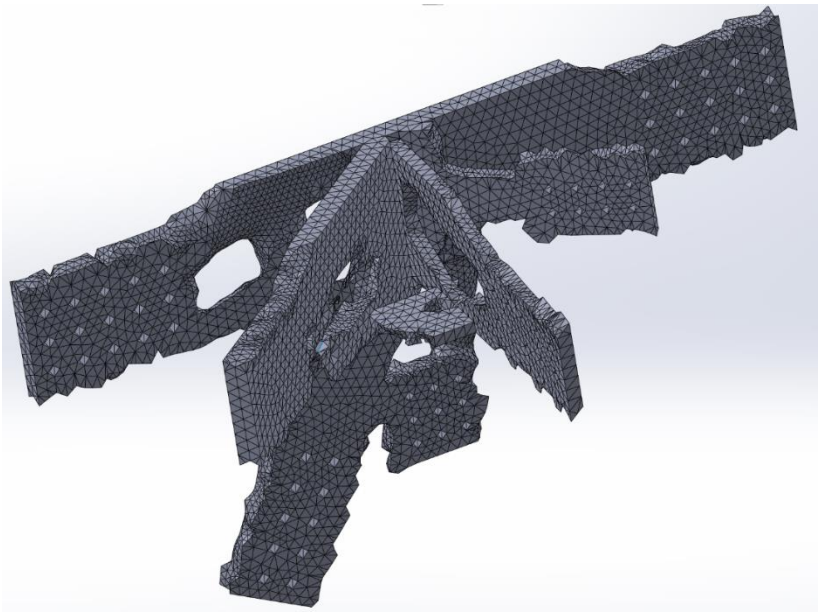

Figure 23. STL of structural node after topological optimization

Planes were created on each flat face, and the mesh was used to outline the shape each plate should be, to accomplish the goal of light weighting the part while maintaining buildability.

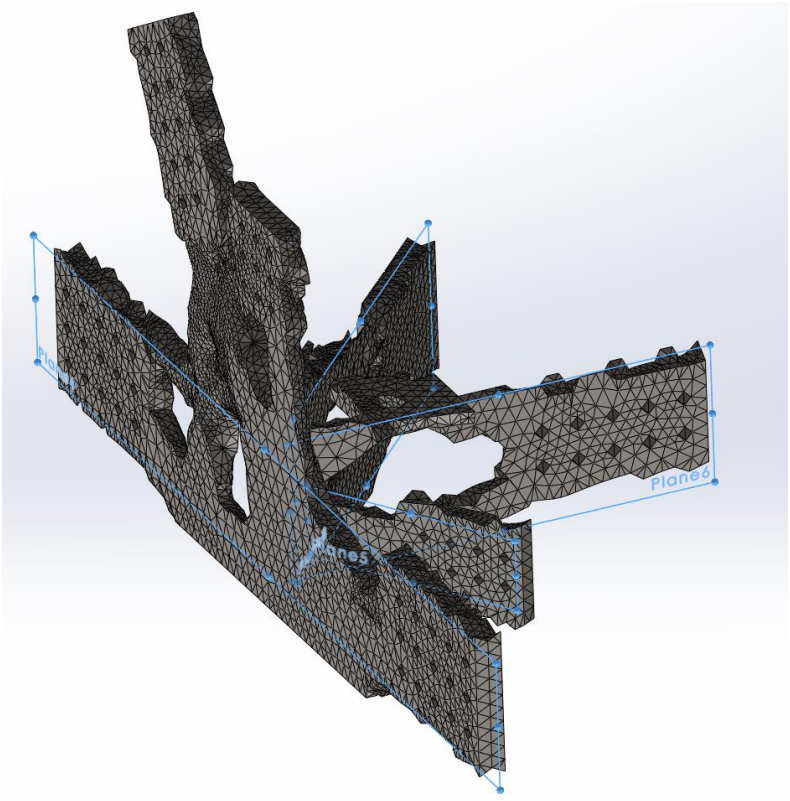

Figure 24. Planes fitted to each to each flat surface of mesh

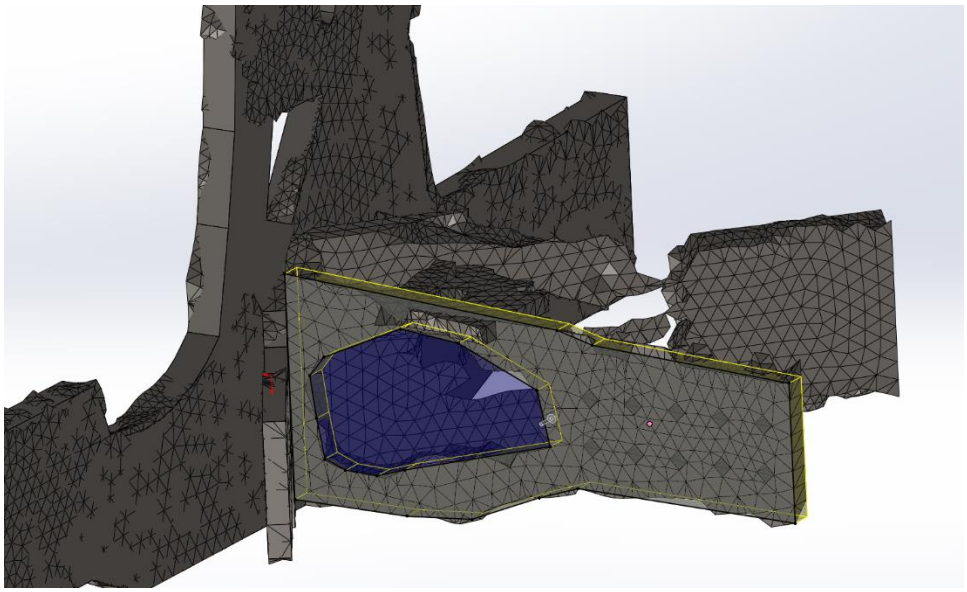

Figure 25. Sketch outlining mesh and extrusion to vertex on opposite face

In Figure 26, the gray mesh is the STL provided by Vestas and the translucent blue body is the cast SN model.

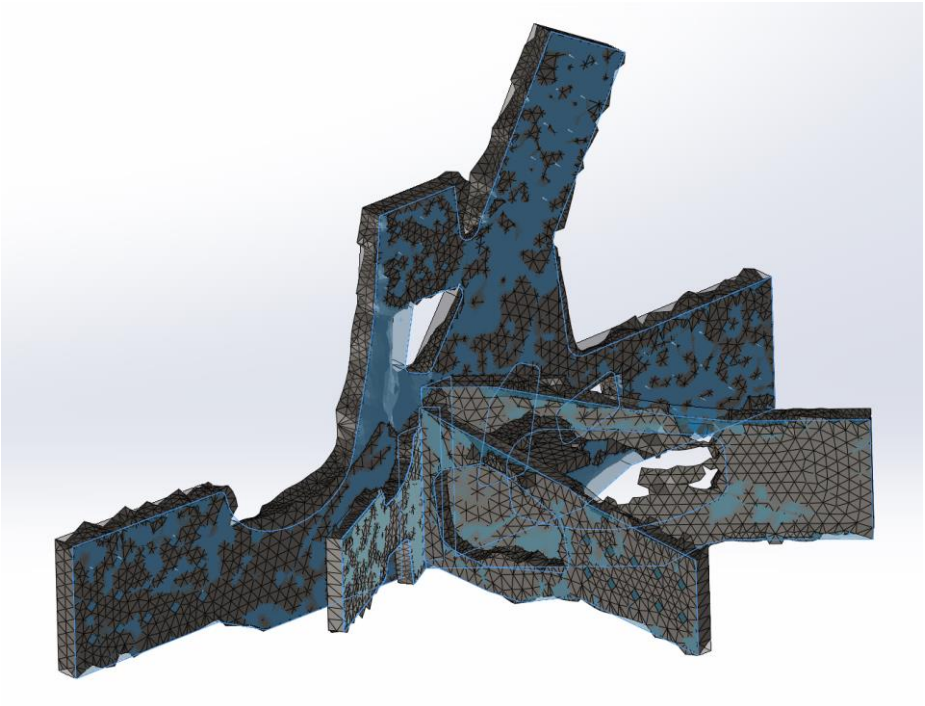

Figure 26. Wrapped to STL

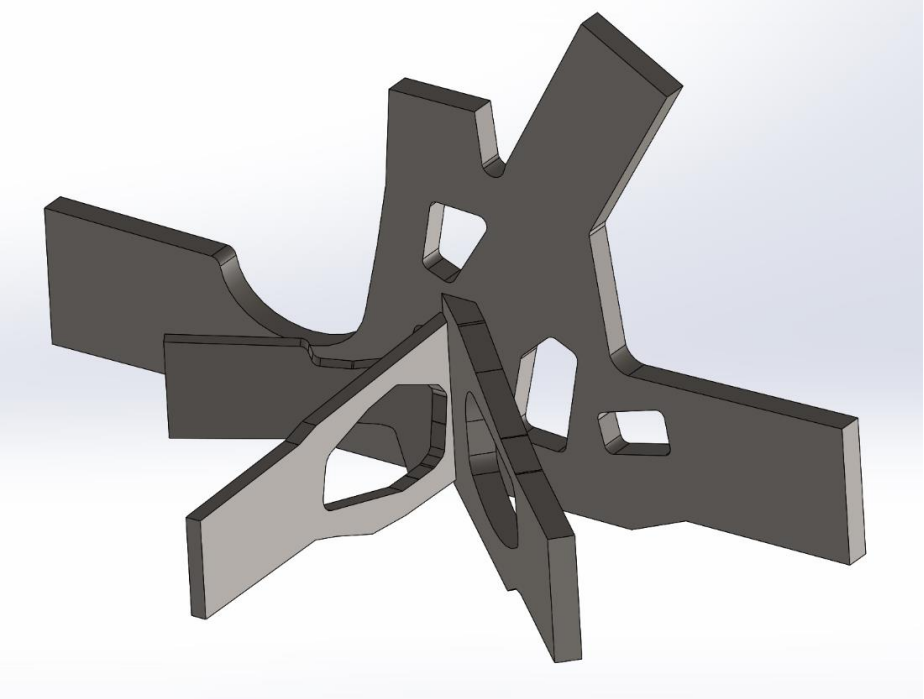

Figure 27. Completed SN Design prior to adding draft angles

In order to cast a part, a draft angle has to be added to every face that is not parallel to the parting line, as shown in Figure 28, so the pattern can be removed from the sand without disturbing the sand mold. The size of the original part has to be increased to account for the shrinkage of the part after solidification and cooling. This part had 3mm added to every surface for shrinkage. The final part is illustrated in Figure 29.

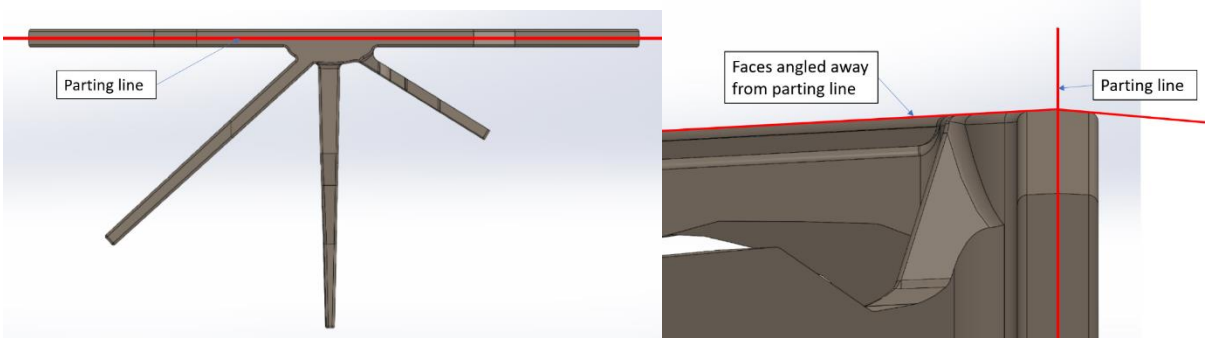

Figure 28. Parting line and draft angles were added to part geometry to facilitate pattern removal from sand

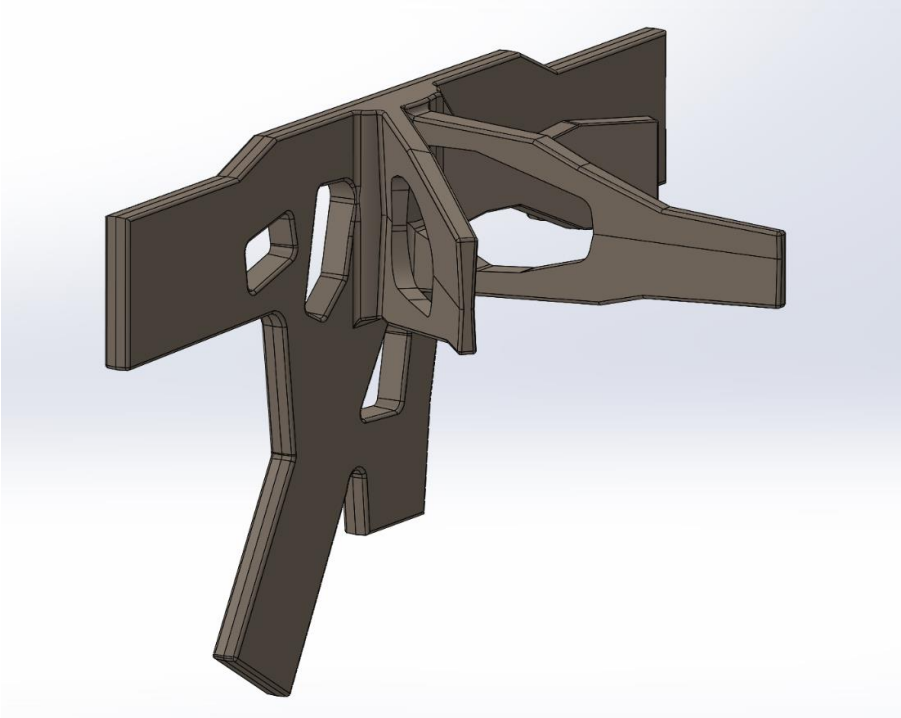

Figure 29. Model of cast bracket with parting line, draft angles, and added material for shrinkage

4.3 Design of Casting Pattern

After the cast part had been designed, a pattern based on this design was printed. As previously described, the top and bottom pattern half of the casing were designed by splitting the part down the parting line and fixing it to a backing plate with locating features.

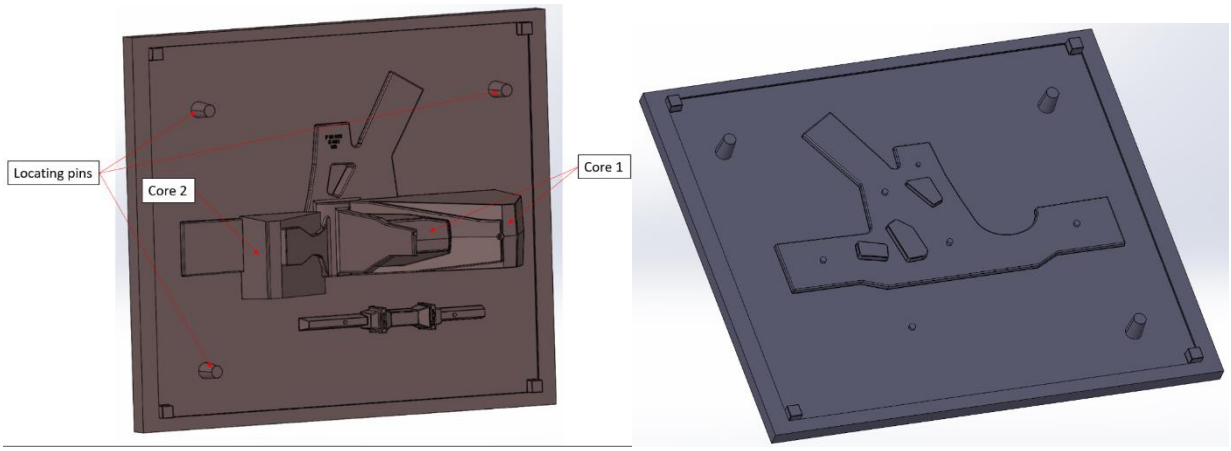

Figure 30. Bottom Pattern for Drag (left) and Top Pattern for Cope (right)

There were sections of the part that were at an angle to the parting plane such that, when creating the mold, sand was removed along with the pattern. So, sand cores were created to fill these voids.

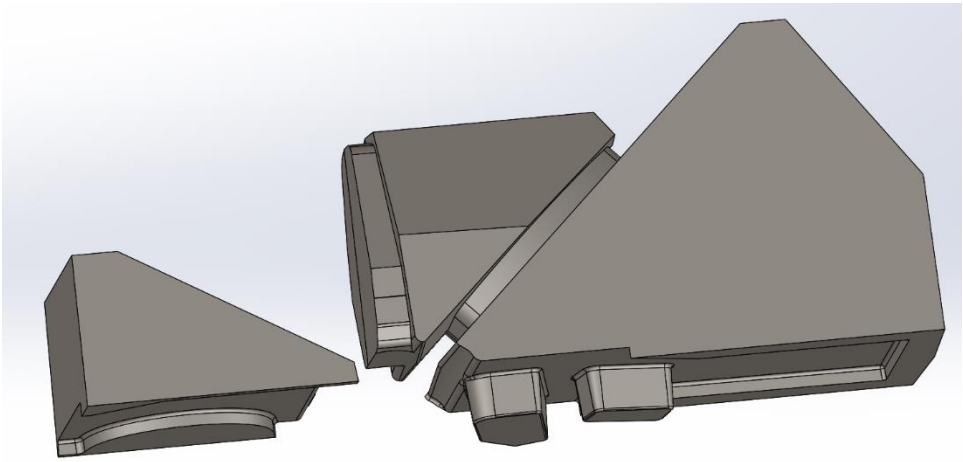

Figure 31. Cores of sand to be inserted into cavities created by pattern in cope and drag.

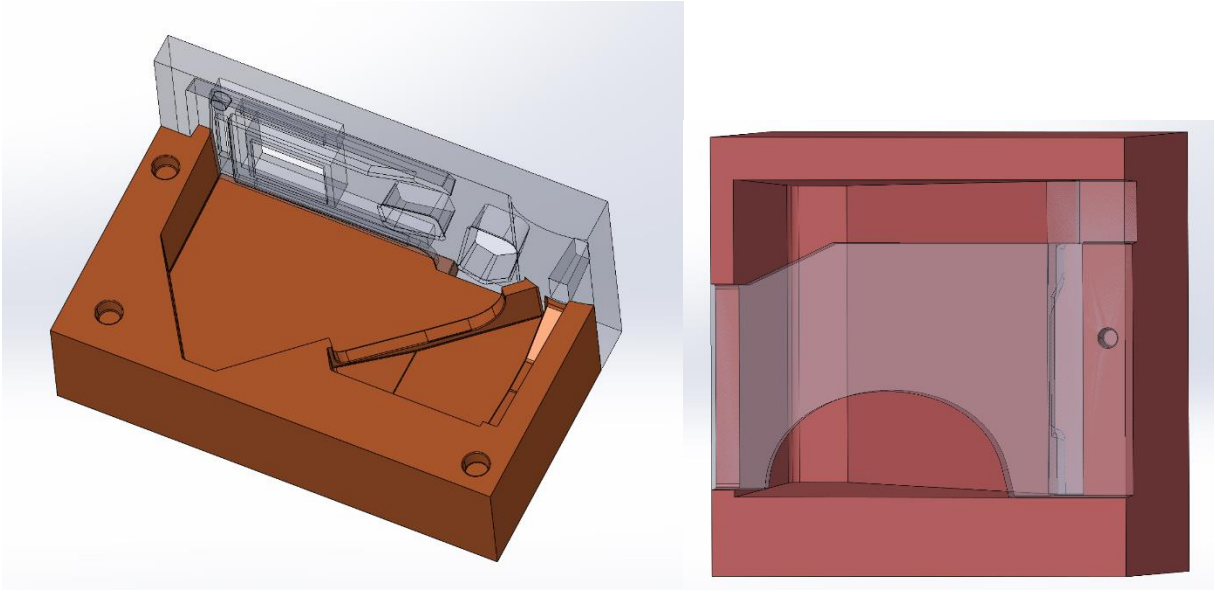

Figure 32. Multi piece core boxes to form cores

4.4 Fabrication

One of the limiting factors in printability is that layer times cannot be too long or too short. When planning to print these parts, there were instances of both too long and too short of layer times. If the back plate of the pattern were printed flat, the layer time would have been over

20 minutes long. This is too much time between layers, which allows the previous layer to cool and thus create a very poor bond between layers. If the plate were printed vertically, the layer times would have been too short, and there would be unprintable overhangs. One solution was to angle the part at a 45-degree angle with breakaway supports underneath. The best surfaces are usually oriented in the Z direction, and for this reason, molds are print on their sides when possible.

Figure 33. Bottom pattern printed at 45 degrees by the CI BAAM

The warping of the bottom pattern was too severe to be used and it had to be reprinted and glued to a plywood sheet to create the pattern back plate, as shown in Figure 34. This decreased the print time from 20 hours to 6 hours and deceased post-processing time by ensuring a flat backer plate that did not need to be machined smooth.

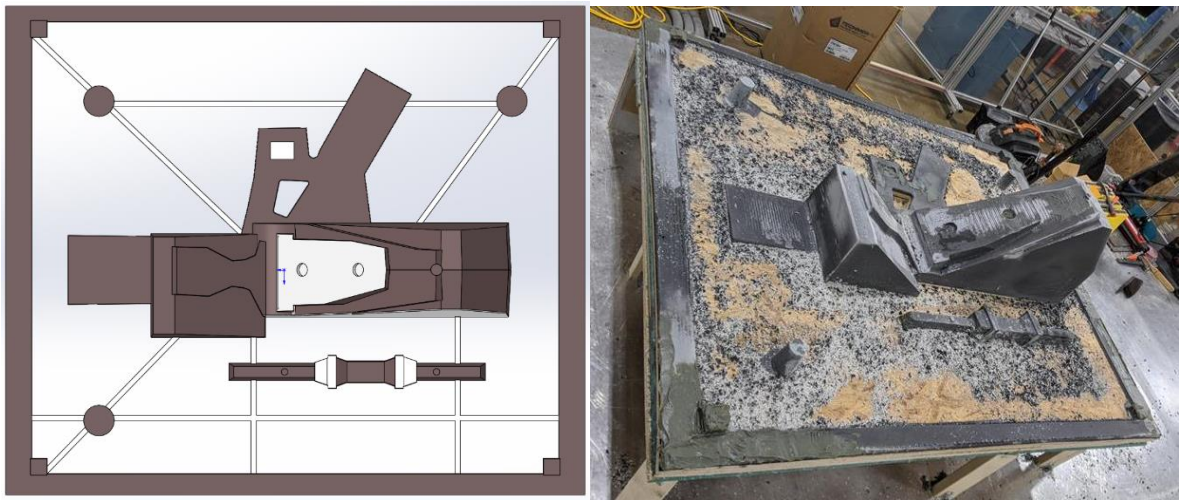

Figure 34. Web printed on BAAM and glued to plywood sheets

The casting house added the sprues, runners, and riser pins to the patterns, based on their expertise, as shown in Figure 35.

Figure 35. Completed bottom pattern with additional flow paths added by casting house

When the cores were placed in the mold, some unintentional gaps were found in between the pattern and the core, shown in Figure 36. Adjustments had to be made by the casting house to make the part fit properly. The cores were slightly larger than intended and material had to be added to the core boxes to make the cores smaller.

Figure 36. Gaps between sand cores and mold

Once the adjustments were made to close the gaps, three SN were cast. There was some leakage at the seam of the parting line and at some of the corners and edges. This material, along with the material that filled the runners and risers, shown in Figure 37, had to be removed after casting.

Figure 37. Cast SN with risers and runners still attached

Some small defects were found in the cast nodes, such as porosity in certain areas, but the parts still performed adequately during testing, despite the defects.

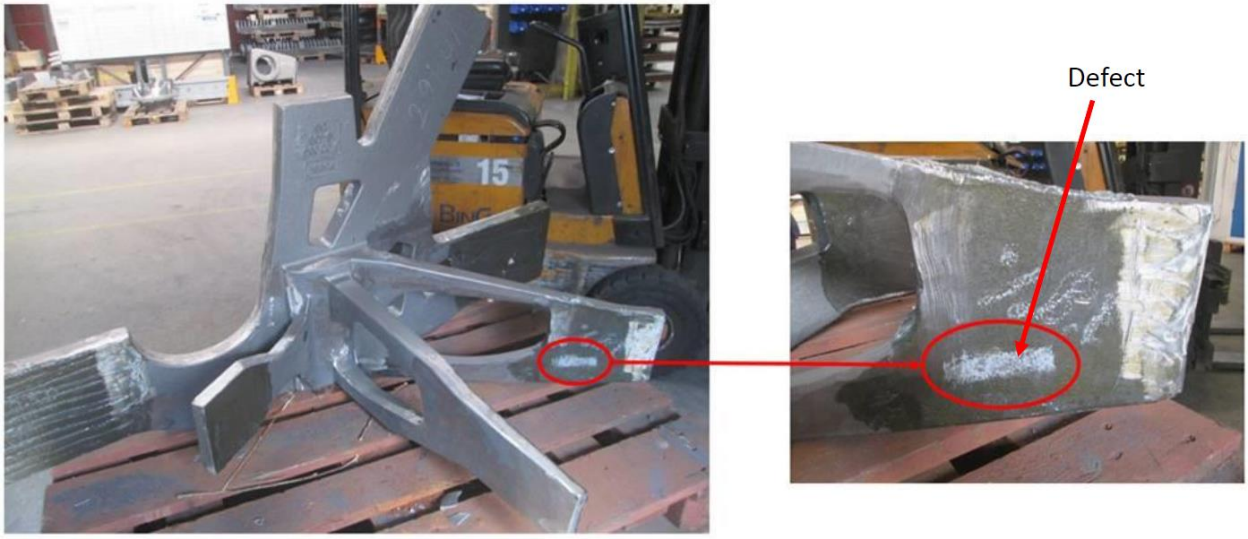

Figure 38. Cast SN after excess material removed

5. ADDITIVE MANUFACTURING OF A TOPOLOGY-OPTIMIZED METALLIC SKELETON NODE

5.1 Manufacturing process: Directed Energy Deposition via MBAAM

Directed energy deposition (DED) uses an intense energy source, such as a laser, electron beam or plasma arc, and selective melting of coaxial feedstock metal in the form of wire or powder to construct a part. Although most applications use metal, other materials such as polymers, ceramics, and composites can be similarly processed. This process family fundamentally differs from powder bed fusion as the feedstock material is selectively deposited only in the path of the energy source. With substantial crossover between these processes and welding techniques, DED applications expand further than part creation to include repair, remanufacturing, and surface coating. The capability to engineer material composition and property gradients in large-scale parts positions DED processes with high potential impact. However, residual stress accumulation in parts due to large thermal gradients can result in distortion and can require additional process steps to relieve stresses. Additionally, a shielding gas, an inert chamber, or a vacuum environment is required to prevent oxidation. DED processes are often combined with subtractive processes in hybrid manufacturing, or parts are manufactured to near-net-shape in the additive process and machined to tolerance in post-

processing. Build volumes on the order of multiple cubic meters are seen, particularly when using wire as feedstock. Processes such as laser deposition welding (LDW), electron beam additive manufacturing (EBAM), laser metal deposition (LMD), laser engineered net shaping (LENS), wire arc additive manufacturing (WAAM), and wire feed metal additive manufacturing fall into the directed energy deposition family [Nycz *et al.*, 2016]. Future innovations in this family include hybrid manufacturing, microstructure control, and large-scale parts.

This project used a WAAM system, called Metal Big Area Additive Manufacturing (MBAAM), to directly manufacture a metallic SN. MBAAM is an advanced arc welding technology developed by ORNL that utilizes robotics and automation, coupled with direct energy deposition, to melt and deposit a wire feedstock in a continuous fashion to build up large-scale metallic structures. The MBAAM manufacturing process utilizes a Wolf Robotics automated gas metal arc welding system. The system is equipped with an ABB IRB 2600 robotic arm (with an IRC5 controller), a Lincoln Electric R500 Power Wave welder, a water-cooled torch, and a dual push-pull wire feeder.

5.2 Design of Printed Component

Initially, there were no constraints or limitations placed on print strategy—all design work was done with the intent of exploring feasibility of printing the part itself. In order to begin design, it was extremely important to understand the intended application of the part. Vestas, a wind turbine solutions and services company, intended to use the part as a bracket that would be independently pulled at each wall of the part. Iterative design and discussion with these parameters in mind led to additional specifications: the part must be dense at the ends of the "arms" of the part, or the walls which branched out, for mounting purposes; the remainder of the arms should not be totally dense to avoid unnecessary material; and light-weighting should be a key focus to demonstrate the capabilities of AM.

To begin the design process, Finite Element Analysis (FEA) data and point cloud data, provided from Vestas, was imported into Solidworks. The FEA provided an "ideal thickness" of the part, and so it was critical to determine a printing material for the final part. By doing so, the part was designed with toolpaths in mind, such that designed part dimensions would produce expected results from the known behavior of the weld beads. Mild steel (Lincoln Electric L-59) was the material of choice. After discussion on the results of the preliminary FEA, it was decided

that the part should be light weighted in the lower stress areas, gusseted between arms that experience large stresses, and a balance between strength and weight should be maintained in all other areas, as shown in Figure 39.

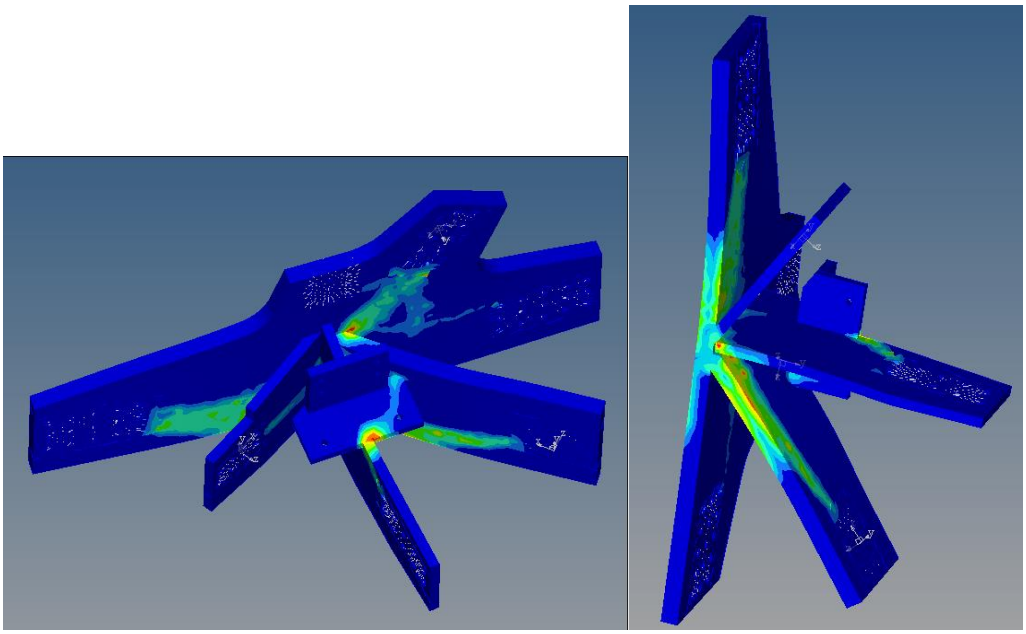

Figure 39. FEA results indication high stress areas in light colors and low stress areas in dark blue

Since each wall of the part was an inch or more in thickness, they were designed with the intent of producing a 2-bead path on either side. There were regular connecting beads across the width, serving as regular gussets for an internal structure similar to the construction of a cardboard wall. Ideally, each bead of mild steel was placed 4.5mm apart, but in reality, each bead had a welded width of over 6mm, meaning that the beads will slightly overlap and combine.

Light-weighted areas were a challenge; light-weighting typically entails material removal in a hole-like manner, but designing a hole within walls of an additive part requires any overhanging material to be built progressively, and so the “hole” must be built more triangularly to be feasible. However, tension applied to a part with triangular holes in the walls would produce stress points, so a new strategy was adopted. Instead of designing large holes in the part for light-weighting in low-stress areas, the walls were thinned in select areas. Imagine pinching a piece of cardboard between fingers: the cardboard becomes thin in the pinched section and smoothly transitions back to the designed thickness elsewhere. This strategy was adopted for the AM design: the part was “pinched” in low-stress sections by slowly bringing each of the two-

bead outer portions of each wall into a single two-bead wall. In this manner, these new light-weight areas used less than half of the material than the typical walls.

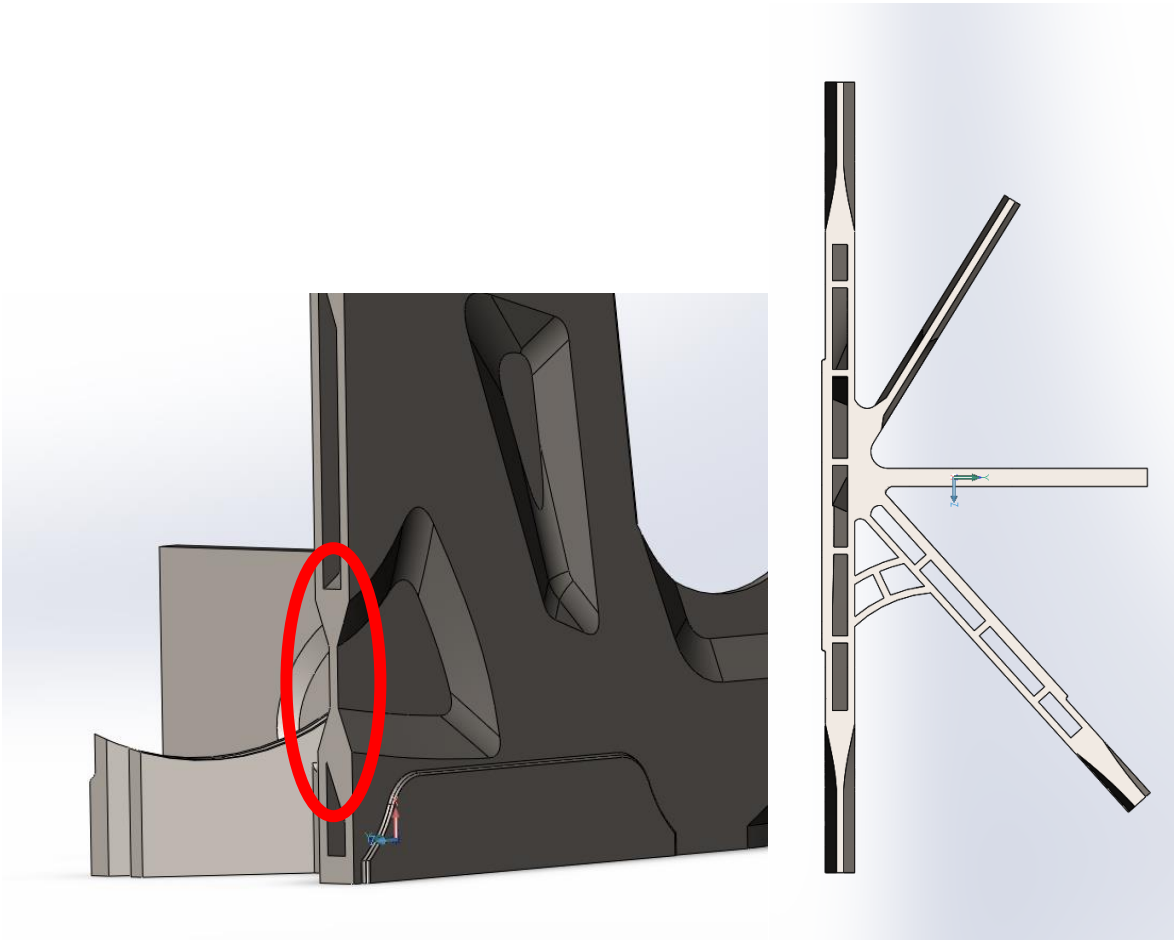

Figure 40. Cross section of designed part showing light-weighted section (left) and wall structure (right)

Final design considerations were standard AM design rules for the developed wire-arc additive process: overhangs must be supported, the required outer surface of the part should be overbuilt by a minimum 3mm to 5mm to minimize the impact of stair-stepped layers on post-processing, and any toolpath corners should be rounded to mimic the real printing process.

5.3 Fabrication

Printed Part Weight: 336lb
Print Time: 115h

Devising a print strategy proved to be another challenge. With a footprint of roughly 1m x 0.4m and a layer geometry which spiders out in multiple directions, the stresses seen in the build plate during the beginning of the print would be high. This is due to the solidification of hot weld material on a cold build plate; the weld material contracts as it cools and can easily curl inch-thick build plates like potato chips. With many walls in different directions, building on a single plate would cause extreme stresses in many directions, and so this idea was discarded. Instead, multiple build plates were trimmed and bolted to a table, following the profile of the part as shown in Figure 41. These were not welded or otherwise attached to one another, as it was assumed that the part printing process would sufficiently join the plates and support the manufactured part.

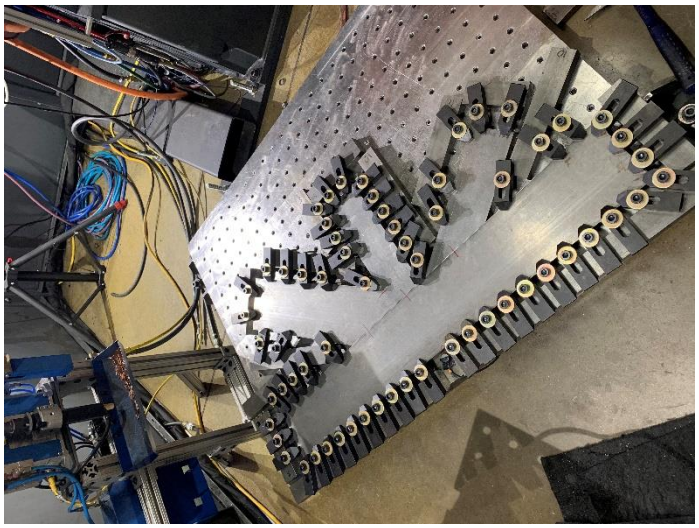

Figure 41. Build plate strategy

The part was then constructed from the L-59 weld wire using a surface tension transfer (STT) weld mode for the detailed outer features, and a spray transfer weld mode for the infill areas. The part began printing on 9/23 at approx. 8am and concluded on 9/28 at approx. 3am. There was one major torch collision on layer 90, which had a check TCP (tool center point) error. Diagnostics were run and proved to be in spec. There was a clear shift at this layer in the part, but no corrective action was taken.

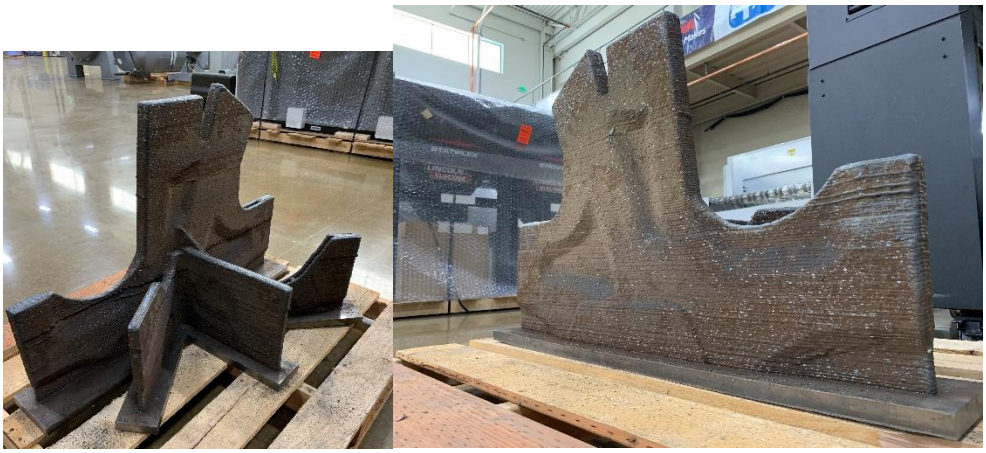

Figure 42. Completed AM Printed Node

Overall, the mild steel STT parameters and mild steel spray settings worked extremely well. No layers or beads were re-run and the part built relatively flat. The multiple-piece base plate showed no abnormal stress concentrations or reasons for concern.

6. TEST RESULTS AND OUTCOMES

6.1 Testing Procedure

The test program was carried out by FORCE Technologies of Aarhus, Denmark.

The test program consisted of:
1) Finite Element Analysis (FEA) of nodes and placing of strain gauges as a result of the analysis
2) Load tests in a test rig for each of the 3 types of AM nodes
3) Load tests of a reference control node provided by Vestas

Once the already-machined nodes were received by FORCE, the mounting holes for the grips had to be drilled and strain gauges had to be mounted. It was decided to make a hole pattern that derived from the pattern on the reference node provided by Vestas as a control. The strain gauges were placed according to the strain gauge plan derived from FEA performed by FORCE Technologies. They were placed in the highest loaded areas and/or areas of special

interest on each node. The surfaces beneath the strain gauges had to be ground and polished to an even surface before gluing on the gauges.

The test load rig design is illustrated by Figure 43, wherein the SN is mounted with hydraulic cylinders mounted to each of the five arms in the vertical plane. The test rig was fabricated by FORCE, and a picture of the experimental setup is shown below in Figure 44.

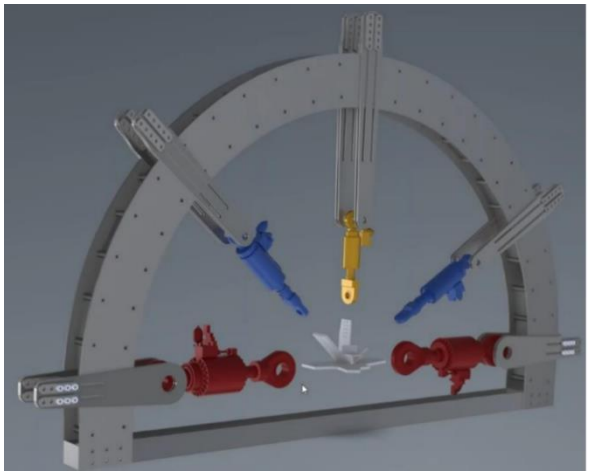

Figure 43. Load rig design from FORCE Technologies

Figure 44. Fabricated Test Rig

As the figure illustrates, two 1600kN actuators were connected to arms 1 and 5, one 250kN actuator was connected to arm 3, and two 350kN actuators were connected to arms 2 and 4 of the specimens. The test setup consisted of FORCE Technology's test rig placed on the strong floor at LCST Component and Structure testing A/S facilities at Lindø. The test rig had an outer diameter

of 4.5m and was designed to withstand the full load of the actuators, but the design loads were below this upper limit.

The test specimens were placed in the test rig, which was adapted to fit the different dimensions and angles of the specimens. Between tests, a crane was used to adapt the actuators to the geometry of the different SNs. Before the nodes entered the test rig, the actuators had to be lined up. Actuators 1 and 5 were supported with wooden blocks and pallets to align them horizontally. The actuators on arms 2 and 4 were each attached to a winch to fix them at the right angles. Spacers were made to ensure a good connection between the friction plates and the arms of the node. When the nodes were sitting in the test rig, a simple structure with two M64 threaded rods and two u-beams were used to restrain the node while under load. One u-beam was placed on the friction plate while another was below the H-beam, and the two were connected by a threaded rod, as seen in Figure 45.

Figure 45. Horizontal Constraint

The tests were executed in the order prescribed in Table 2. The initial prototype composite node was used to evaluate the test rig (signals, data acquisition etc.), but the test data is not presented in this report because of improper ramp rates that were tuned for the remainder of the tests.

Table 2. Test Specimen Order and Design Loads

Order	Name
1	Prototype
2	Composite_V02_1
3	Composite_V02_2
5	Cast_1
6	Cast_3
7	Cast_2
8	AM 3D printed Metal
9	Reference

Arm	*Design load [kN]*
1	40
2	25
3	25
4	25
5	40

When a node was placed in the test rig, all signals were checked before zeroing forces and strain gauges. The hydraulic pump unit (HPU) was started in high pressure prior to starting the test itself. The test sequence is listed below:

1) Actuators 1-5 ramp to 0kN within a 30 second period
2) Actuators 1-5 ramps to design loads within a 180 second period and hold the load for 10 seconds
3) Actuators 1-5 ramp to 0kN within a 30 second period
4) Steps 2 and 3 are repeated two additional times
5) Step 2 is repeated, and force is maintained for 10 seconds
6) Actuators 1-5 ramp from design load towards 400kN (on actuators 1 and 5) and 250kN (on actuators 2, 3 and 4) with the same strain rate as the previous ramps.
7) Test end if any limit is violated or the test operator shut down

During the tests, the test operator monitored values and a video recording. Eventually, the operator would stop the test when an actuator ran out of displacement. In the tests where the node failed, the program automatically shut down, but in all other tests it was shut down by the operator. It did not make sense to try and fail the metal nodes, as it would have required more force than the actuators could deliver at the displacement available. Thus, the tests were stopped when loads were around 250kN (arm 1 and 5)/156kN (arms 2, 3 and 4) or when one actuator ran out of displacement.

6.2 Test Results

6.2.1 Sparse Fill Hybrid Composite Node

The V1 hybrid composite node failed on the backside of arm 1 before reaching design load specifications. The loads on arms 1 and 5 were around 25kN while loads on arms 2, 3 and 4 were around 14kN when the node failed. Before failure, arms 1 and 5 reached 62.5% of the design loads, and arms 2, 3 and 4 reached 56% of the design loads. Data from the V1 hybrid composite node test is shown in Figure 46.

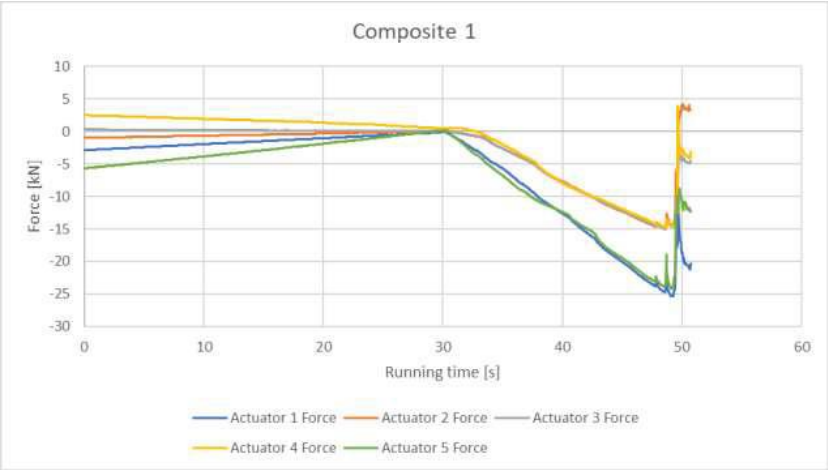

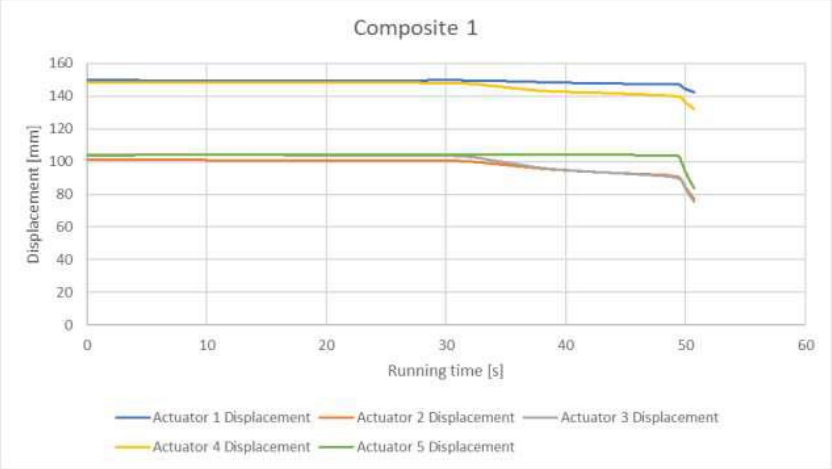

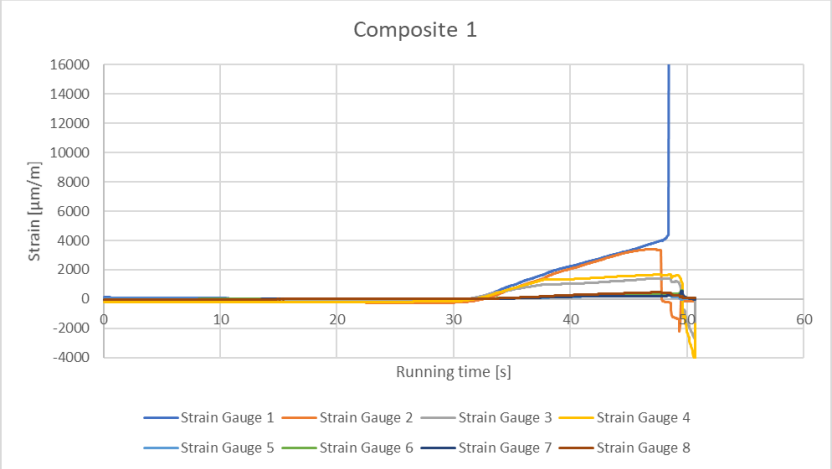

Figure 46. V1 Composite node test data

Failure of the node occurred at stress concentrator in the grip section at the transition between machined and as printed flange.

6.2.2 Hollow Core and Fill Hybrid Composite Node

Arm 5 of the V2 hybrid composite node failed and separated, and arm 4 cracked, before reaching design load specifications. The loads on arms 1 and 5 were around -20kN while loads on arms 2, 3 and 4 were around -12kN when the node failed, i.e. close in magnitude, but slightly lower than V1. The node failed at the interface between the machined flange and as-printed transition. This is shown in Figure 47 and Figure 48 like the previous composite SN test.

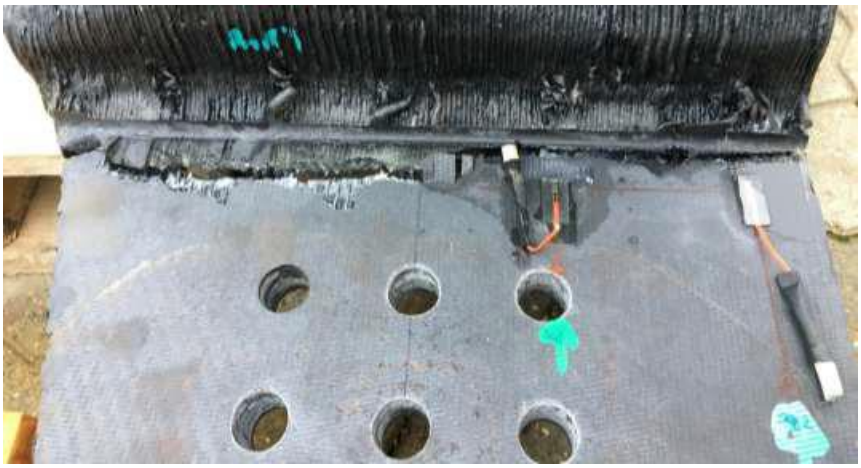

Figure 47. Composite V2 node failure Arm 5

Figure 48. Composite V2 node failure Arm 4

The data for composite node V2 is shown in Figure 49.

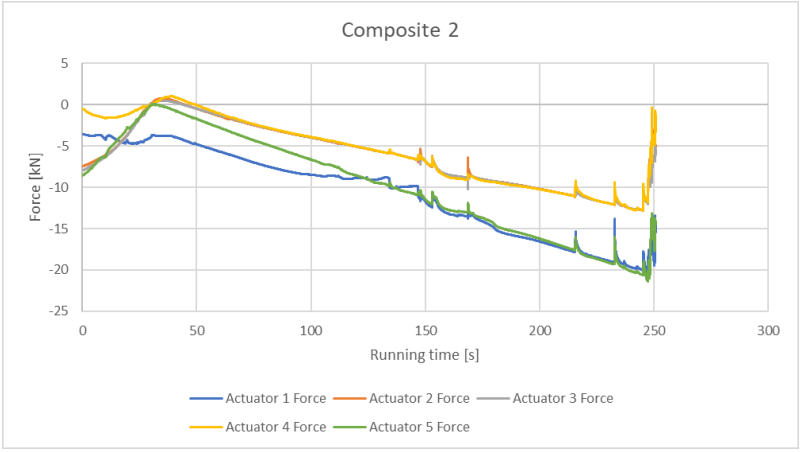

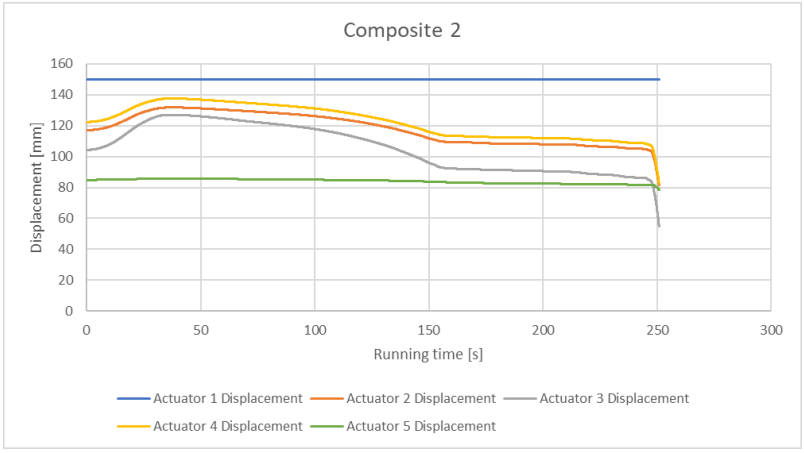

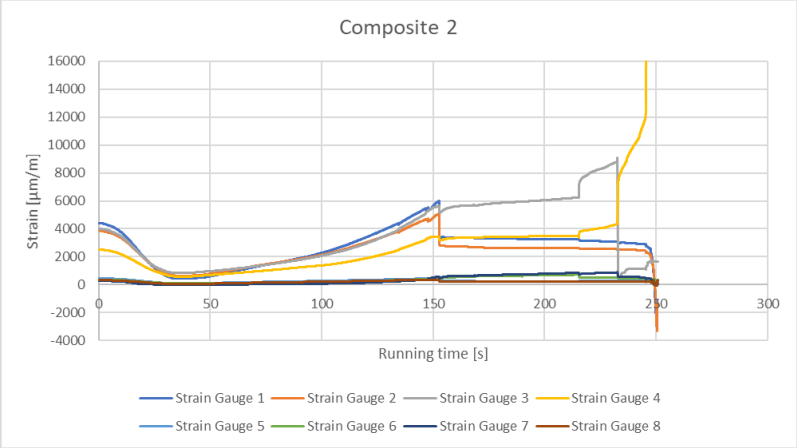

Figure 49. V2 Composite node test data

6.2.3 Cast Skeleton Nodes

The cast node reached design loads without any problems and with no plastic deformation. Cast 1 was ultimately loaded to 195kN (for arms 1 and 5) and 121kN (for arms 2, 3, 4). Cast 2 was loaded to -268kN and -168kN for the same respective arms. Cast 3 was loaded to -252kN and -159kN, also for the same respective arms. These loads only induced plastic deformation; the test ultimately ended when actuators ran out of travel. Note this is greater than 4.8x the design load without material failure. The nodes were slightly deformed but intact after the test.

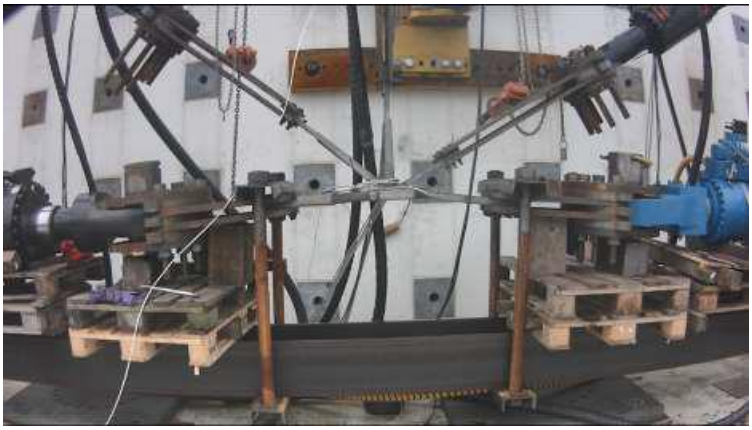

Figure 50. A cast node during testing

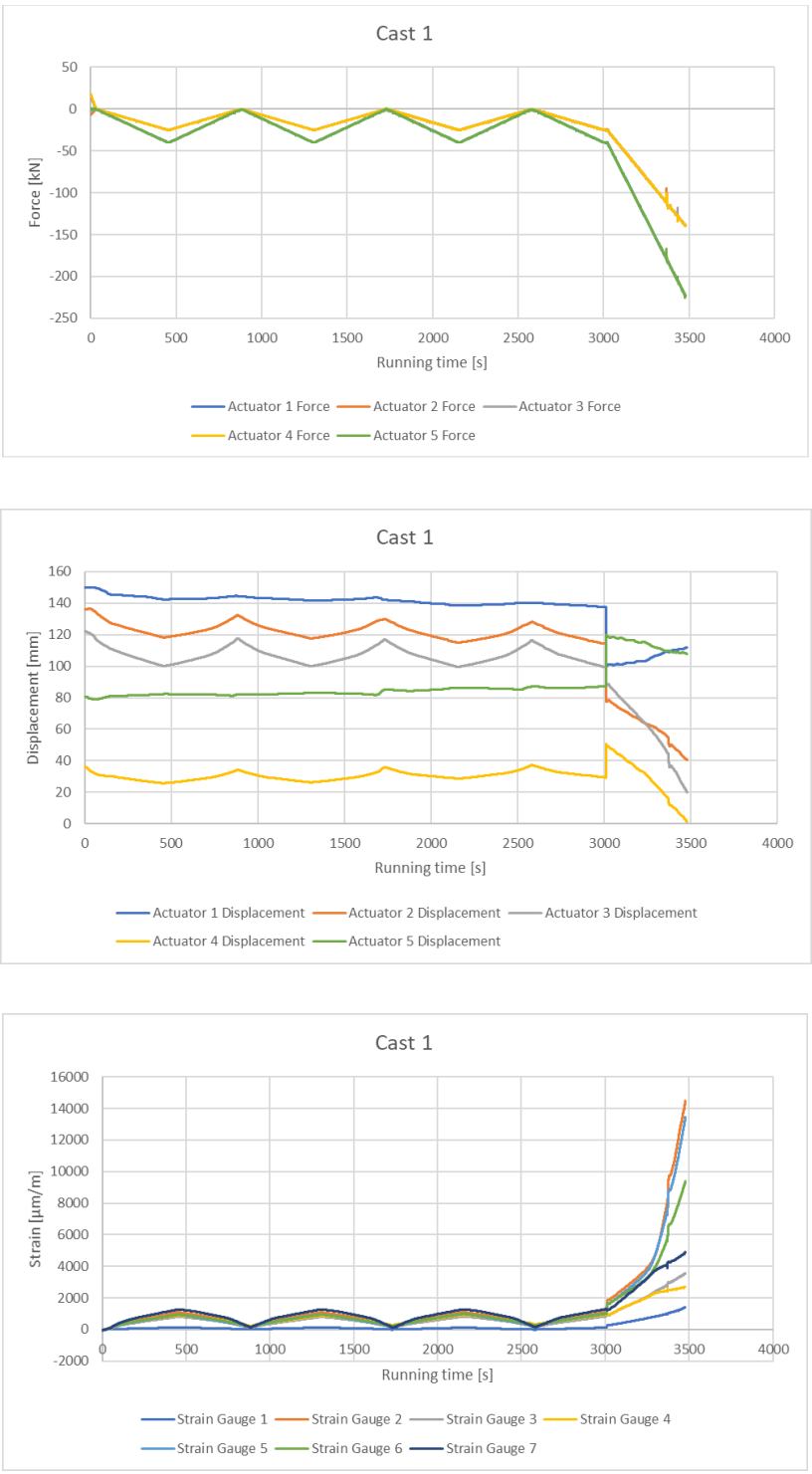

Figure 51. Example cast node test data

6.2.4 Direct Metal AM Printed SN

Like the cast node, the direct metal printed AM node reached design loads without any problems and no plastic deformation. The node was ultimately loaded to 280kN for arms 1 and 5, and 175kN for arms 2, 3, and 4, at which point only plastic deformation was induced. Again, the test ultimately ended when actuators ran out of travel. Note this is greater than 7x the design load without material failure. The node was slightly deformed but intact after the test.

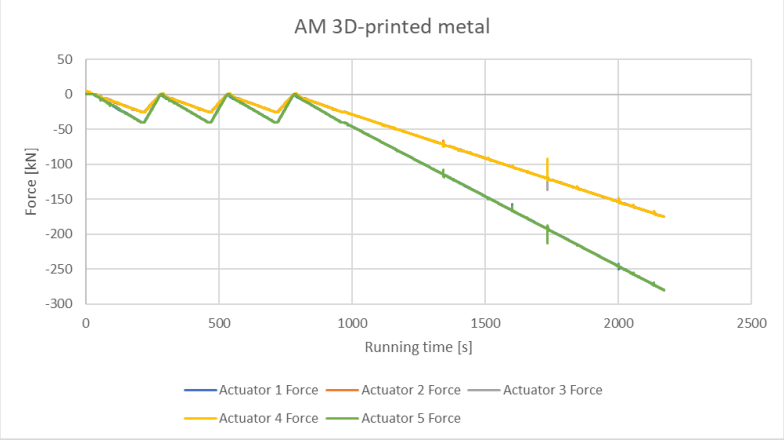

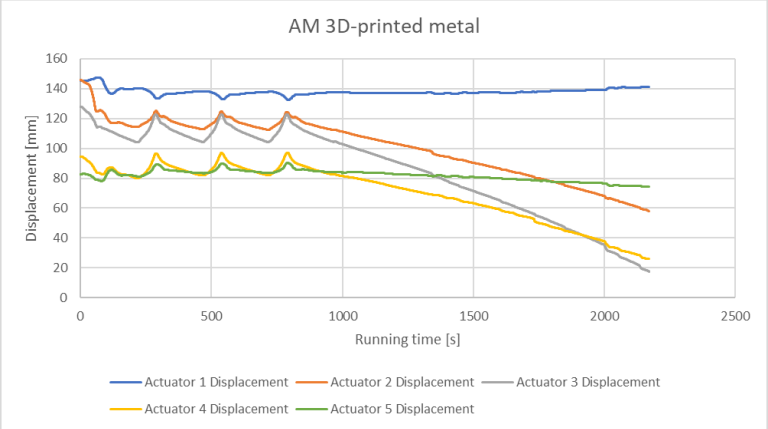

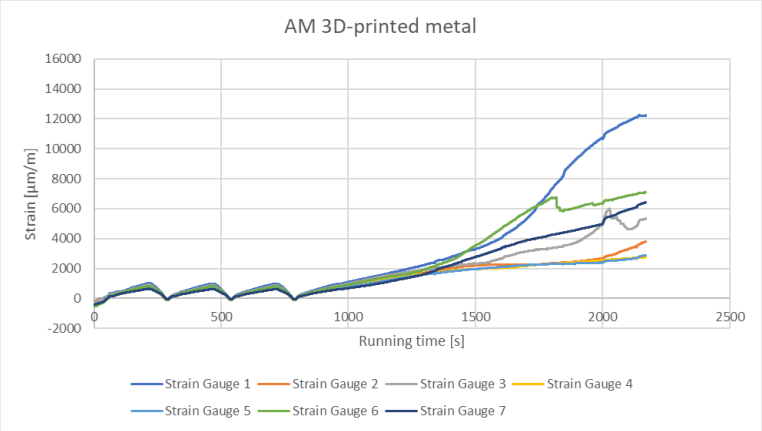

Figure 52. Data from direct printed AM node test

6.2.5 Reference/Control Conventional Production Node

The tested conventional reference node reached design loads without any problems and no plastic deformation. The node was ultimately loaded to 357/172kN (respectively arms 1, 5 and arms 2, 3, 4).

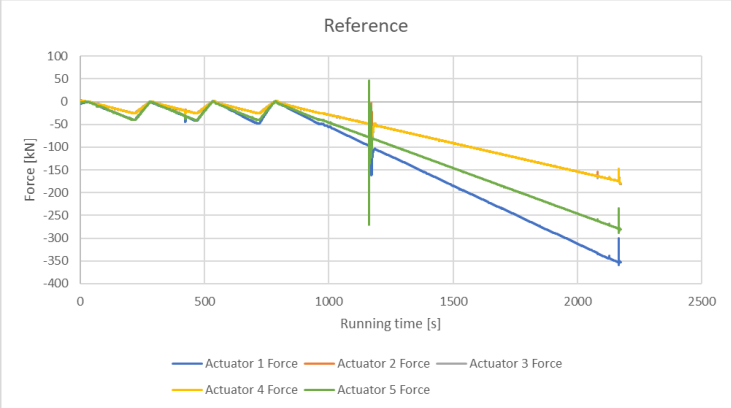

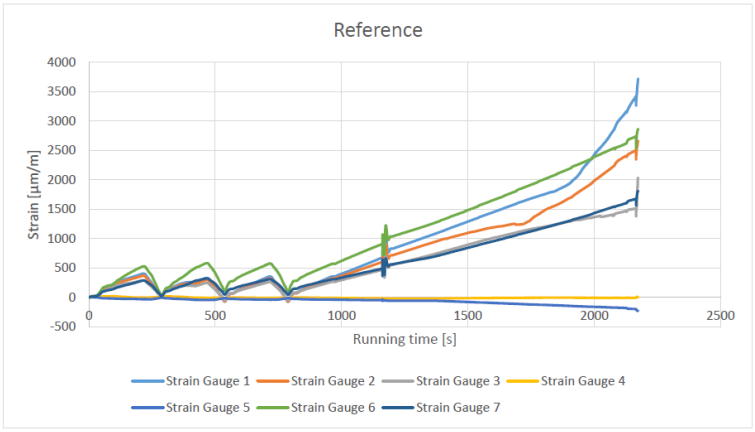

Figure 53. Reference node testing data

6.2.6 Testing Conclusions

As noted in the preceding sections, all the metallic node variations met the design criteria, with the direct and indirect AM processes proving equally valid and performing favorably when compared to the conventionally produced SN. The composite nodes experienced material failure below the design loads, but compare favorably on a specific strength basis, as they weigh less than ½ the weight of the lightest metallic node. With the additional weight budget, it seems entirely possible that a composite node could be created with a wider flange section that would meet the designed loading criteria, but further research and testing would be required.

7. TECHNOECONOMIC ANALYSIS

A technoeconomic analysis was conducted to investigate the economic feasibility of all the approaches discussed above. First, a technoeconomic profile of the process currently used to construct the SN was

compiled as the profile of the “baseline part”. Then, each process investigated in this project was also profiled and compared to the baseline part. The results are summarized below.

7.1 BASELINE PART

The baseline structure, shown in Figure 54, measures 1.395 m X 0.682 m X 0.812 m (4.57 ft x 2.24 ft x 2.66 ft) and has a mass of 328.6 kg (724.4 lb). The part is comprised of a multitude of laser-cut S355 structural steel plates that are manually welded together with a full-penetration weld to form the final product. The production cost to manufacture this part using conventional laser-cutting and manual welding processes is estimated at $3.00/kg ($1.36/lb), based upon Vestas supplier data, manufacturing in India, and the use of S355 structural steel plate. The prototype cost to manufacture this part however is significantly higher due to factors such as tooling costs and low-volume production. Prototype cost is estimated at $7.50/kg ($3.40/lb) for this part, or 2.5 times higher than production costs, based upon discussions with Vestas. With a part mass of 328.6 kg (724.4 lb), the total production cost using conventional manufacturing processes is estimated at $985.80, while the prototype cost is estimated at $2,464.50.

Figure 54. Baseline structural steel part.

For both production and prototype components, the lead time from receipt of the final drawing to receipt of first article is estimated at 13 weeks, assuming transport from India to Denmark. This timeframe assumes ocean freight as the lowest cost transport solution. Decreasing lead times either through local sourcing or through air transport will incur significant cost increases either through labor charges or transport charges and is not considered at this time.

7.2 BAAM – CF-ABS COMPOSITE PARTS

This section discusses the efforts to use the BAAM system to reproduce the baseline structural steel part as a topology-optimized composite part. There are three major components of the total production cost: material costs, machine costs, and labor costs. These are independently summarized below.

Material costs are directly impacted by the feedstock used to print the part. For the CF-ABS20 used in this study, the feedstock cost is estimated at $11.02/kg ($5/lb). The total feedstock material cost is based on the mass of the 3D printed part. The first iteration (Part 1) had an estimated print volume of .03130 m^3 (1.1054 ft^3) and a mass of 81.70 kg (180.12 lb) when filled with epoxy. The second iteration (Part 2) had an estimated print volume of .02737 m^3 (0.9665 ft^3) and a mass of 81.94 kg (180.65 lb) when filled with epoxy. Therefore, the total feedstock cost was $698.43 for Part 1 and $672.62 for Part 2. Consumable material costs, such as the build plate and nozzle purge material, were estimated at $75.00 per build. The cost of the epoxy material used to reinforce these parts is estimated at $5.00/kg ($2.27/lb). Again, the total cost is dependent on the volume of the internal cavity. The internal cavity volume of Part 1 was estimated at .03835 m3 (1.3544 ft3), resulting in an epoxy mass of 46.0 kg (101.5 lb) and an epoxy cost of $230.10. The internal cavity volume of Part 2 was estimated at .04228 m3 (1.4932 ft3), resulting in an epoxy mass of 50.7 kg (111.9 lb) and an epoxy cost of $253.70. Thus, the total material cost is estimated to be $698.43 for Part 1, and $672.62 for Part 2.

Machine costs are directly impacted by the time it takes to completely build the part. The maximum deposition rate on the BAAM system with current extruder technology is 22.68 kg/hr (50.00 lb/hr). However, due part complexities associated with topology optimization and infill patterns, these three parts experienced much slower deposition rates. The average deposition rate was estimated to have been 5.00 kg/hr (11.02 lb/hr). The print time was estimated to be 7.13 hours for Part 1 and 6.23 hours for Part 2. In addition to the 3D print times, an estimated 2

additional hours were necessary for machine set-up and print bed warming, and an estimated additional 1 hour was necessary for part removal during post-processing of each print. The time for epoxy processing was estimated to be 1 hour for preparation and 3 hours for cure, but operational costs for epoxy fill application were assumed negligible and were thus not included. Operational costs for the BAAM were estimated at $150/hr, based upon an estimated machine cost of $1,500,000 and other associated operating expenses. For Part 1, a cycle time of 10.13 hours resulted in an estimated operational cost of $1520.46. For Part 2, a cycle time of 9.23 hours resulted in an estimated operational cost of $1386.05. Here, cycle times include pre-processing, processing, and post-processing operations.

BAAM labor rates were estimated at $35.00/hr and are based on the U.S. Bureau of Labor Statistics hourly wage data for machinist skillsets, which is approximately $25/hr but was multiplied by a 1.4 cost burden multiplier. Labor costs assume one laborer is required for all BAAM and epoxy fill processes. The 14.13 hours of total labor for Part 1 was estimated at $494.55. The 13.23 hours of total labor for Part 2 was estimated at $463.16.

The total costs of the parts, including materials, operations, and labor, were estimated at $2,713.66 for Part 1 and $2,522.09 for Part 2. For both parts, the prototype and production part costs are assumed the same. Comparing total part costs, Part 2, which is the 3D printed CF-ABS shell filled with epoxy resin, had the lowest cost of the three parts considered. The cost of Part 2 is very comparable to the baseline welded-steel prototype cost ($2,645.50), but over 2.5 times higher than the baseline welded-steel production cost ($985.80). Comparing timeframes, 13.23 (for Part 2) is roughly 40 times faster than the estimated 13-week lead time to receive the welded-steel plate part from a supplier in India, assuming a 40-hour work week. This initially indicates that BAAM technology could be a viable alternative for prototype development. However, considering the relatively low strength of composite and epoxy in comparison to structural steel, the technology would be better suited to functional prototypes over direct structural steel replacements.

7.3 BAAM – SAND CASTING PATTERNS AND CORE BOXES

This section discusses the effort to use the BAAM system to reproduce the baseline structural steel part as a metal casting in which the sand-casting patterns and cores are 3D printed from CF-ABS. The material, machine and labor costs for this approach are detailed below.

The feedstock material used in this approach was the same as the feedstock discussed in the previous section (CF-ABS), and thus the feedstock cost is the same. The total volume of the 8 parts was estimated at 0.6870 m^3 (24.2611 ft^3) with an estimated mass of 783.2 kg (1,726.7 lb). The total feedstock cost for all 8 parts was estimated at $8,633.07. Consumable material costs, such as the build plate and nozzle purge material, were estimated at $75.00 per build, or $600.00 for all 8 parts. Thus, the total material cost for the 8 parts with consumables was estimated at $9,233.07.

The total BAAM operational time to 3D-print the 8 individual parts was 93.06 hours, based upon 69.06 hours of print time and 24 hours of pre- and post-processing time. Additional post-processing steps were required and involved moving the parts from the BAAM to the Thermwood 5-axis CNC router to further finish the surface, drill, and index the patterns and cores. It was estimated that each part required an additional 2 hours for part setup and indexing, and 1 hour for part removal from the Thermwood. The material removal rate for surfacing was estimated at 9677.4 mm^2/min (15.0 in^2/min). The surfacing area on the top pattern was estimated at 3,662,855.0 mm^2 (5,677.4 in^2), requiring an estimated 6.3 hours. The surfacing area on the bottom pattern was estimated at 4,886,588.0 mm^2 (7,574.2 in^2), requiring an estimated 8.4 hours. The surfacing area on core box 1 was estimated at 4,370,636.0 mm^2 (6774.5 in^2), requiring an estimated 7.5 hours. The surfacing area on core box 2 was estimated at 1,345,929.0 mm^2 (2086.2 in^2), requiring an estimated 2.3 hours. The total surfacing time for all 8 parts on the Thermwood was thus estimated at 24.6 hours, and the total time to process the parts on the Thermwood, including part setup and removal, was estimated at 48.6 hours.

Operational costs for the BAAM were estimated at $150.00/hr, as previously discussed. Operational costs for the Thermwood were estimated at $50.00/hr, based upon an estimated machine cost of $500,000.00 and other associated operating expenses. Operational costs for 93 hours and 4 minutes on the BAAM machine were thus estimated at $13,960.00, and operational costs for 48.57 hours on the Thermwood machine were estimated at $2,430.00; total operational costs were estimated at $16,390.00.

Labor costs assumed one laborer is required for all BAAM and Thermwood machine processes and was assessed at a labor rate of $35/hr, as previously discussed. Therefore, the cost of labor for the BAAM machine time (93.07 hours) was estimated at $3,257.33, while the cost of

labor for the Thermwood machine time (48.57 hours) was estimated at $1,699.92; total labor costs were estimated at $4,957.16.

The total pattern and core box cost, including materials, operations, and labor, was estimated at $30,578.29. The final prototype costs are derived by amortizing the costs of the 3D-printed pattern and core box, and a $780.28 pattern test article, over 3 parts. The final prototype part cost is thus estimated to be $11,233.13, which includes $10,192.76 in 3D-printed pattern costs, $260.09 in pattern test article costs, $708.33 in EN-GJS-400-18-LT material costs, and $71.94 in non-destructive inspection (NDI) costs. Similarly, final serial production costs are derived by amortizing the costs of the 3D-printed pattern, core box, and pattern test article over 500 parts, to approximate serial production level costs. The final serial production part cost is thus estimated to be $842.99, which includes $61.16 in pattern costs, $1.56 in pattern test article costs, $708.33 in EN-GJS-400-18-LT material costs, and $71.94 in non-destructive inspection (NDI) costs.

In comparison to the baseline welded plate structure, the prototype production costs of this approach, at $11,233.13, are 4.25 times higher than the baseline prototype cost, at $2,645.50. On the other hand, the serial production costs of this approach, at $842.99, are 1.17 times lower than the baseline production cost of $985.80. However, before conclusions on the economic feasibility of this approach can be drawn, the traditional method of making patterns and core boxes from wood must also be considered. Traditionally, the patterns and core boxes used in the sand-casting process are commonly manufactured from wood by either a skilled pattern maker or a CNC router machine. This analysis assumes a skilled pattern maker is used. The baseline casting costs were derived from a casting house contracted to manufacture the prototype articles for this project, which was Uldalls Jernstoberi, A/S, based in Vejen, Denmark. The costs were converted from DKK to USD using an exchange rate of 6.00, an approximate 10-year median exchange rate. The cost to manufacture the wooden patterns and core boxes was $14,166.67, of which $13,386.00 was allocated to pattern making and $780.27 was allocated to a final pattern test article and inspection. The final cost to manufacture three metal castings for the project, based on traditionally manufactured wooden patterns and core boxes, cast iron material, and non-destructive inspection (NDI), was estimated at $16,507.50, or $5,502.50 per casting.

Using the same methods to calculate the prototype and serial production costs, the traditionally manufactured prototype costs were estimated to be $5,502.50, and the traditionally

manufactured production casting was estimated to be $808.61. The prototype and serial production costs of the baseline part, traditionally manufactured pattern cast part, and 3D-printed pattern cast part are summarized in Figure 55.

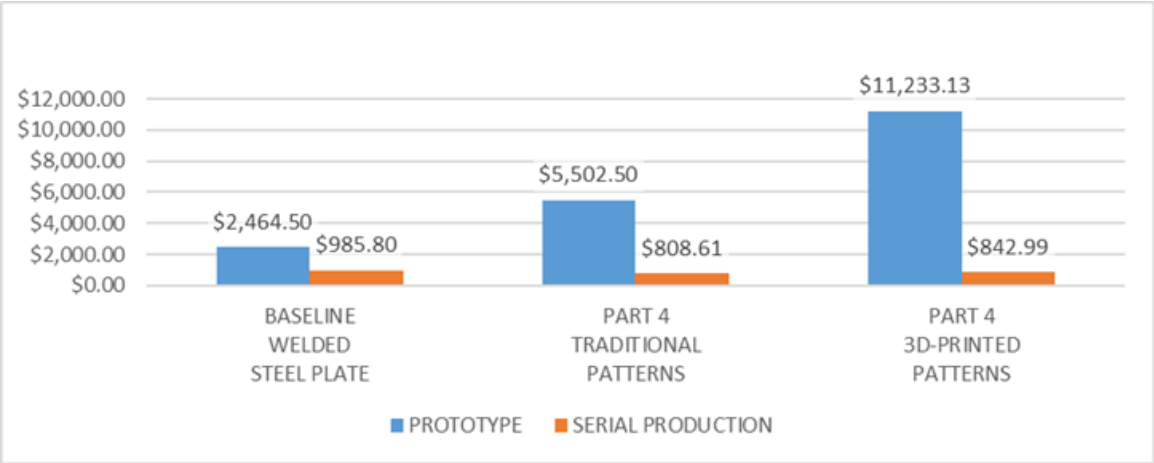

Figure 55. Part costs using traditional wooden and 3D-printed patterns and core boxes.

As illustrated in the figure, at both the prototype and serial production level, the 3D-printing approach was found to be more expensive than the traditional pattern-making method. Therefore, this approach does not demonstrate a clear economic advantage over either metal castings that utilize traditionally manufactured patterns and cores, or over the baseline welded plate structure. This is not to say that additive manufacturing is not a viable alternative in the metal casting space. There may be opportunities for the BAAM system when considering part complexity, lead times, pattern storage costs, and lost-foam castings. Alternatively, there are other technologies in this space, such as the ExOne S-Max, that take an entirely different approach, bypassing pattern making altogether, and directly 3D-printing the mold in sand. Directly 3D-printing sand casting molds is an interesting additive manufacturing technology that is not considered in this analysis but should be considered in future work.

7.4 MBAAM – METAL PART

This section discusses the reproduction of the baseline structural steel part utilizing metal BAAM (mBAAM). This part geometry differs from the composite and cast nodes previously discussed, as well as the baseline welded plate structure, in that it is smaller, as shown in Figure 16. The net effect is that comparisons will be proximate, not direct. A directly comparable

mBAAM part would be estimated to cost approximately 10% more. The material, machine and labor costs of this approach are summarized below.

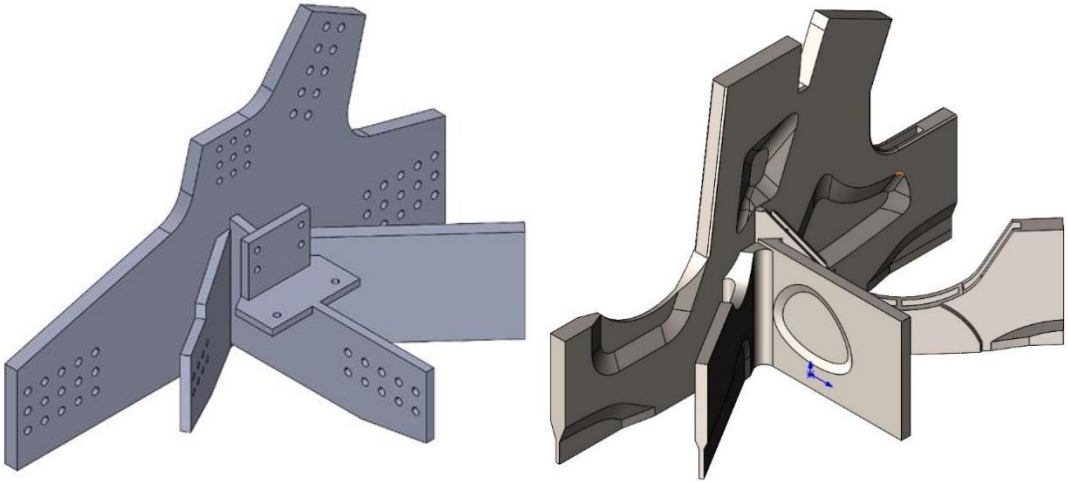

Figure 56. Smaller geometric footprint of the mBAAM part (shown on the right) compared to the baseline part (shown on the left).

SUPERARC l-59, a mild steel wire, was used as the feedstock in this approach. The material cost for the steel wire feedstock was estimated at $6.61/kg ($3.00/lb). The material cost for the steel base plate was estimated at $4.41/kg ($2.00/lb). Thus, the material cost of the as-printed 336.8 kg (742.5 lb) mBAAM part was $2,227.55, and the cost of the 58.9 7kg (130.0 lb) non-reusable base plate was $260.00, for a total material cost of $2,487.55. The mass of the final as-printed mBAAM part is higher than the as-designed CAD mass due to the weld bead dynamics and inherent overbuild, but removal of the excess material with a secondary subtractive manufacturing process is not considered in this analysis.

Manufacturing the part on the mBAAM system, from start to finish, was completed in 115 hours of continuous operation. In addition to the print time, an estimated 2 additional hours were required for machine set up and print bed warming during pre-processing, and another 2 additional hours were required for part removal during post-processing. Therefore, the total machine time is estimated to have been 119 hours. Operational costs for the mBAAM are estimated at $50.00/hr, based upon an estimated machine cost of $500,000.00 and other associated operating expenses. 119 hours of mBAAM machine time thus has an operational cost estimated at $5,950.00. The labor costs assumed one laborer is required for all mBAAM

processes and were assessed at a higher rate than that used for BAAM and epoxy operations, resulting in a total estimated labor cost of $5,950.00.

The total MBAAM part cost, including materials, operational expenses, and labor, was thus estimated at $14,387.55. Prototype and production part costs are assumed the same for the mBAAM process. Therefore, when comparing estimated final part costs for traditional vs. additive manufacturing, the mBAAM manufactured part cost ($14,386.25) is over 5 times higher than the baseline welded-steel prototype cost ($2,645.50) and over 14 times higher than the baseline welded-steel production cost ($985.80). On the other hand, when comparing timeframes, 119 hours, or just under 5 days to manufacture the MBAAM part, is approximately 95% faster than the estimated 13-week lead time to receive a welded-steel plate part from a supplier in India.

On a cost basis, the higher costs of the MBAAM part would be hard to justify, especially when considering the production costs of the baseline welded-steel part. However, there may be certain scenarios where the high costs could be outweighed by factors such as reduced lead times, or the ability to manufacture in-house or locally. For example, the ability to shorten the prototype lead time by upwards of 95% to either meet or accelerate prototype or certification schedules could justify the increased cost. Or, considering that express air-shipment of such large steel parts from suppliers in Asia to Europe or the US could cost in the hundreds of thousands, not only could the higher part cost be justified, but capital investment in a MBAAM machine, estimated at $500,000.00, could even be justified.

7.5 FUTURE SCENARIOS

As additive manufacturing technologies continue to advance at a rapid pace, it is important from a strategic and investment perspective to assess future potential alongside current potential. Two future scenarios are considered which assume continued investment and research. A near-term future scenario increases the average deposition rate to the current maximum deposition rate, reduces feedstock costs by 50%, reduces operational costs by 50%, and assumes feedstock material defects or weaknesses are eliminated through scientific and technical advances. The far-term future scenario expands upon the near-term scenario by increasing the average deposition rate by a factor of ten and eliminating labor costs through full automation. Only the

BAAM-printed casting pattern and mBAAM approaches were considered in future scenarios, because the directly manufactured composite parts failed during load testing.

For the BAAM-printed casting pattern approach, the near-term future scenario assumes an average deposition rate of 45.36kg/hr (100lb/hr) [8], CF-ABS20 feedstock cost of $5.51/kg ($2.5/lb), operational cost of $75/hr, and interlaminar z-direction strength deficiencies are solved. The far-term future scenario further assumes an average deposition rate of 453.59kg/hr (1000lb/hr) [12], and no labor costs. The BAAM near-term future costs are thus estimated to be $5,468.44 for prototype and $808.41 for serial production, and the far-term future costs are estimated to be $4,031.87 for prototype and $799.79 for serial production. While the projected future cost reductions for the BAAM approach are impressive, but when compared against traditional pattern making costs, there does not appear to be a business case for future investment in this manufacturing strategy.

For the mBAAM approach, the near-term future scenario assumes an average deposition rate of 6.80kg/hr (15lb/hr) [13], steel wire feedstock cost of $3.31 ($1.5/lb), operational cost of $25/hr, and welding defects are solved. The far-term future scenario further assumes an average deposition rate of 68.04kg/hr (150lb/hr), and no labor costs. The mBAAM near-term future costs are thus estimated to be $5,386.34 and far-term future costs are estimated to be $1,597.52, for both prototype and serial production. These future cost reductions demonstrate a large potential for the mBAAM technology. The far-term projected future costs are extremely competitive and on par with the current baseline welded plate structure costs. Factor in the ability of mBAAM technology to 3D-print advanced designs and light-weighting strategies that are not economically feasible with current manufacturing processes, and investment in mBAAM technology could fuel future advancements in large-scale recyclable metallic wind turbine structures.

7.6 CONCLUSION

A detailed techno-economic analysis of three additive manufacturing processes concludes that conventional welding of steel plates is found to be the most cost-effective manufacturing method to produce the large structural steel part considered in this analysis. However, certain scenarios were identified where the higher cost of utilizing additive manufacturing technologies may be justified. Of the additive manufacturing technologies analyzed in this report, MBAAM technology is identified as the most promising technology considering factors such as, current

economics, potential future technical advances and cost reductions, and the ability to 3D print full strength steel.

8. BIBLIOGRAPHY

[1] Atzeni, Eleonora, and Alessandro Salmi. "Economics of additive manufacturing for end-usable metal parts." The International Journal of Advanced Manufacturing Technology 62.9-12 (2012): 1147-1155.

[2] A. Elliott and C. Waters, Additive Manufacturing for Designers: A Primer. 2019.

[3] Chesser, Phillip C., et al. “Using Post-Tensioning in Large Scale Additive Parts for Load Bearing Structures.” Solid Freeform Fabrication Symposium, 2018, pp. 556–67.

[4] Greer, Clayton, et al. “Introduction to the Design Rules for Metal Big Area Additive Manufacturing.” Additive Manufacturing, vol. 27, no. N/A, 2019, pp. 159–66, doi:10.1016/j.addma.2019.02.016.

[5] Hughes, Gordon. "Why is wind power so expensive." Global warming policy foundation (2012).

[6] Love, Lonnie, et al. “Commercialization of Big Area Additive Manufacturing .” ORNL Report , BT-, vol. ORNL/TM-20, 2020.

[7] Love, Lonnie J. et al. (2014), "The importance of carbon fiber to polymer additive manufacturing," Journal of Materials Research 29.17: 1893-1898.

[8] Nycz, A., et al. “Large Scale Metal Additive Techniques Review.” Solid Freeform Fabrication Symposium, 2016, pp. 2001–06, https://sffsymposium.engr.utexas.edu/sites/default/files/2016/161-Nycz.pdf.

[9] Roschli, Alex et al. (2019), "Designing for big area additive manufacturing," Additive Manufacturing, Vol. 25: 275-285.

[10] Roschli, Alex, et al. “Increasing Interlaminar Strength in Large Scale Additive Manufacturing.” Solid Freeform Fabrication 2018: Proceedings of the 29th Annual International Solid Freeform Fabrication Symposium - An Additive Manufacturing Conference, SFF 2018, vol. 29, 2020, pp. 543–55.

[11] Otarawanna, S., Dahle, A.K., (2011),”Casting of aluminum alloys”, *Fundamentals of Aluminum Metallurgy*, Woodhead Publishing Series in Metals and Surface Engineering, pp. 141-154

[12] Post, Brian, et al. “Additive Manufacturing of Wind Turbine Molds”, ORNL report, 2017

[13] Post, Brian et al. (2) (2017) The Current State of Additive Manufacturing in Wind Energy Systems. United States: N. p. 10.2172/1415918.

[14] Hassen, Ahmed et al. (2020). “Scaling Up Metal Additive Manufacturing Process to Fabricate Molds for Composite Manufacturing.” *Additive Manufacturing*. 32. 101093. 10.1016/j.addma.2020.101093.